Fakultät für Physik der

Technischen Universität München

Electrical characterization of colloidal Au particles on functionalized nanogap electrodes

Master Thesis

von

Rocío Murcia

Walter Schottky Institut

Lehrstuhl für experimentelle Halbleiterphysik

Prof. Dr. G. Abstreiter

August 2007

Table of Contents

Abstract

Abstract

In this thesis nanogap electrodes are fabricated using a novel concept for metal electrodes with about 20 nm separation for electrical conductance measurements. The devices were fabricated from custom-made four inch diameter Silicon On Insulator (SOI) wafers comprising a 5 μm thick top silicon layer (resistivity 1–10 Ω cm) which is separated from the 400 μm bulk silicon handle wafer by a thin buried silicon dioxide layer of 20 nm width. All preparation steps involve only standard silicon or SOI microelectronics process technology. After cutting the wafer into 9 × 9 mm^2 sample pieces, plateau-like mesa structures are formed by conventional optical lithography and two subsequent reactive ion etching (RIE) steps. In the next step, the accessible buried oxide is selectively recess-etched in 5% hydrofluoric (HF) acid solution. Due to the extremely high selectivity of HF in etching silicon oxide versus silicon, a gap having near the size given by the buried oxide layer thickness is formed. An additional, third RIE etching step was applied following the wet etching to smoothen the exposed Si sidewalls. Afterwards, contact pads (Ti /Au) are deposited by e-beam evaporation on top of the plateau structures, as well as down in the etched plane close to the plateau, as pads for wire bonding. Finally, the actual nanogap electrodes are formed by a thin film deposition step, with typical metal thickness of a few nanometres. The thin film is evaporated from a 45° angle in order to cover simultaneously both the plateau top surface and the nanogap side on the plateau wall.

SOI wafers have been selected because of their suitable properties for further biological applications. The main advantage that SOI wafers present is that the nanogap geometry is predefined by the Buried Oxide (BOX) layer. Another clear advantage is also that we can apply the Standard Silicon Technology (SST) for the whole nanogap processing. During fabrication only SST without any high-resolution nanolithography techniques is employed and the vertical concept allows an array-like parallel processing of many individual devices on the same substrate chip. As analyzed by cross-sectional Transmission Electron Microscope (TEM) analysis the devices exhibit well-defined material layer architecture, determined by the chosen material thicknesses and process parameters.

To investigate the fabricated nanodevices molecules are placed on the nanoelectrodes by means of a self- assembly monolayer (SAM) process, and for bridging the 26 nm nanogap width, we place gold nanoparticles of different sizes in diameter, using a positive AC dielectrophoresis force. The directed assembly of nanoparticles and nanoscale materials onto specific locations of a surface is one of the major challenges in nanotechnology. In the method applied in this thesis an alternating current is used to create a gradient of electrical field that attracts particles in between the two leads used to create the potential. Gold nanoparticle assembly is achieved when dielectrophoretic forces exceed thermal and electrostatic forces and therefore the suitable parameters for this assembly have to be found. Through the development of this thesis a thorough study of trapping experiments is carried out.

After the achievement of a two-junction system (Au/Molecule/Au/Molecule/Au) transport measurements are carried out in the devices. A thoroughly study of I-V characteristics is also developed in the thesis and by means of the result analysis, effects such as Coulomb blockade and variation of the Coulomb blockade staircase are studied.

Chapter 1

_____

Introduction and Motivation

Nanoscience and technology are fields that focus on the development of synthetic methods and surface analytical tools for building structures and materials, typically on the sub-100 nanometer scale, the identification of the chemical and physical consequences of miniaturization, and the use of such properties in the development of novel and functional materials and devices. If one thinks of the established disciplines in terms of a Venn diagram (Figure 1.1), where each scientific and engineering discipline is described by a circle within the diagram, nanotechnology is not an independent, isolated circle but rather one that overlaps all of the existing circles and will continue to grow as the field is developed. It is a field fueled by novel tool developments that will impact and change almost every conventional scientific and engineering subdiscipline by providing new ways of fabricating or synthesizing structures with well-defined and tailorable properties through control over nanoscale architectures [1].
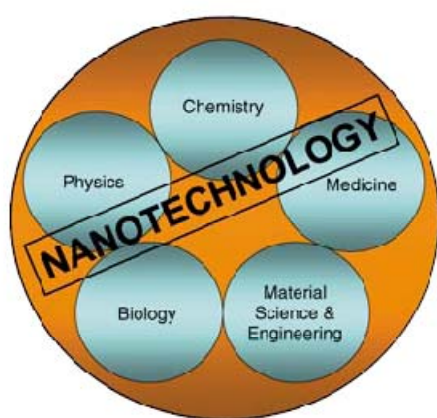
Figure 1.1 Nanotechnology encompasses all fields: New and traditional subdisciplines play their hand in modern nano and micro science and technology [1].

As conventional silicon-based technology approaches its expected physical limits, researchers are exploring molecule based electronics to continue miniaturization of device size and meeting in this way Moore's law (1965) [3]. According to this law the transistor density of semiconductor chips would double roughly every 18 months and therefore the miniaturization of these chips will reach physical limits; for example if the dimension of a device is in the order of a few atoms, one impurity would cause a remarkable effect.

Building an electronic device using individual molecules is one of the ultimate goals in nanotechnology. To achieve this it will be necessary to measure, control and understand electron transport through molecules attached to electrodes. Substantial progress has been made over the past decade in topics such as molecular wires, two terminal switches and diodes, three-terminal transistor-like devices and hybrid devices that use various different signals to control electron transport in molecules [2]. To create a useful device, molecules must be electrically wired to the outside world reliably by electrodes. It is known that the conductance of a molecule is sensitive, not only to the nature of the chemical bonds between the molecule and probing electrodes, but also to the atomic-scale details of the molecule–electrode contact geometry. Precise control of the contact geometry down to the atomic scale has been a difficult challenge. A widely used method is to attach molecules terminated with thiol groups to gold electrodes.
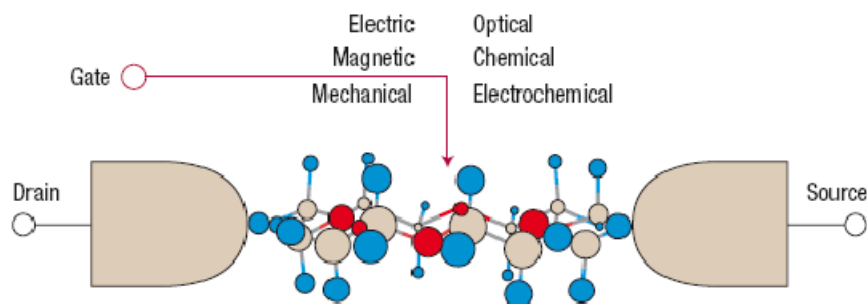
Figure 1.2 Illustration of a single molecule attached to two electrodes as a basic component in molecular electronics. To reach the ultimate goal in device applications, experimental techniques to fabricate such an electrode–molecule–electrode junction and theoretical methods to describe the electron transport properties must be developed [2].

One of the major challenges is the preparation of well defined contacts, often termed nanogap electrodes, which allow one to reliably contact and electrically investigate molecules of a given size. Nanometre spaced electrodes have till the moment been realized by different techniques such as: STM method, where the surface acts as one electrode and the tip of a scanning probe microscope (STM) or an atomic force microscope (AFM) acts as the opposite electrode. Mechanically controlled junctions, where a notched gold wire is exposed to a surface active molecule solution while it was broken, the molecules with thiol endgroups bind covalently to the gold wire and I-V characteristics can be observed after moving the tip together until at least one molecule can bridge the gap and bind to the other tip. Other possibilities are: fabrication of monomolecular films sandwiched between two metallic contacts where the upper one is deposited by evaporation, fabrication based on the nanopore concept and electromigration techniques [4, 5].

Our project can be framed within the vertical nanogaps fabrication techniques using semiconductor layers. As an example of these vertical nanogap electrodes we find the one supported by a group III-V semiconductor heterostructures. In this method, using molecular beam epitaxy a thin gallium arsenide (GaAs) layer is embedded in between two aluminium gallium arsenide (AlGaAs) layers with monolayer precision. By cleaving the substrate an atomically flat surface is obtained exposing the AlGaAs–GaAs sandwich structure. After selectively etching the GaAs layer, the remaining AlGaAs layers are used as a support for deposited thin film metal electrodes [3].

In this thesis nanogap electrodes are fabricated by a novel concept for metal electrodes with about 20 nm separation for electrical conductance measurements [6]. Silicon-on-insulator (SOI) material with 20 nm buried silicon dioxide serves as a base substrate for the formation of SOI plateau structures which, after recess-etching the thin oxide layer and subsequent metal thin film evaporation, feature vertically oriented nanogap electrodes at their exposed sidewalls. SOI material has been selected because of its suitable properties for further biological applications. The main advantage that SOI wafers present is that they predefine our nanogap geometry by the buried oxide layer. Another clear advantage is also that we can apply standard silicon

technology (SST) for the whole nanogap processing. During fabrication only SST without any high-resolution nanolithography techniques is employed and the vertical concept allows an array-like parallel processing of many individual devices on the same substrate chip. As analyzed by cross-sectional TEM analysis the devices exhibit well-defined material layer architecture, determined by the chosen material thicknesses and process parameters.

To investigate the fabricated nanodevices we place molecules on the nanoelectrodes by means of a self- assembled monolayer process, and for bridging the 26 nm nanogap width, we place gold nanoparticles of different sizes in diameter, using a positive AC dielectrophoresis force. The directed assembly of nanoparticles and nanoscale materials onto specific locations of a surface is one of the major challenges in nanotechnology [7]. In the method applied in this thesis an alternating current is used to create a gradient of electrical field that attracts particles in between the two leads used to create the potential. Gold nanoparticle assembly is achieved when dielectrophoretic forces exceed thermal and electrostatic forces. After the achievement of a two-junction system transport measurements are carried out in our devices. A thorough study of I-V characteristics is also developed in the thesis.
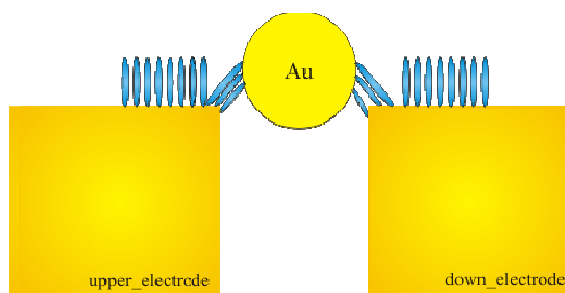
Figure 1.3 Schematic of our system. Two nanometer spaced electrodes, with a molecule covering layer and a bridging Au nanocolloid trapped between the two leads; creating a so called two-junction system (Au/molecule/Au/molecule/Au).

This thesis is organized as follows: after this introduction the used experimental techniques and methods during this work are described in chapter two. Subsequently, chapter three introduces to more detail the process for the silicon on insulator nanogaps fabrication. The theory and experimental work carried out for metallic nanoparticles positioning is presented in chapter four. And in the final chapter, the transport measurements carried out in our two junction system are exposed and analyzed.

Chapter 2

Experimental setup and methods

In the first part of this chapter two instruments for the nanostructure characterization such as the scanning electron microscope (SEM) and the transmission electron microscope (TEM) are briefly discussed. Furthermore the test measurement point system and the setup for low temperature conductance measurements are introduced.

In the last part of the chapter the concept of reactive ion etching (RIE) and the RIE machine operation, used in our sample processing, are explained.

2.1 Methods for sample characterization

The scanning electron microscope (SEM), as well as the transmission electron microscope TEM, assuming a very simplified model, operate on the same basic principle as the optical microscope but use electrons instead of light. These microscope techniques use electrons as light source since electron wavelength is pretty lower comparing with light, as a result a great resolution, in the order of one thousand times better than with an optical microscope, is achieved.

An electron source at the top of the microscope emits electrons that travel through vacuum in the column of the microscope. Instead of glass lenses focusing the light in the optical microscope, electromagnetic lenses are used to focus the electrons into a very thin beam.

2.1.1 Scanning Electron Microscope

The scanning electron microscope (SEM) is used for the investigation of the nanogap devices in our experiments. This microscope is the most widely used of all electron beam instruments, since it is very versatile, and has an excellent spatial resolution. The SEM is a mapping device, rather than an imaging one; this means that the sample is probed by a beam of electrons scanned across the surface.

The electron beam is generated by a filament, most commonly made by a tungsten hairpin gun. This filament is a loop of tungsten which functions as the cathode. A voltage is applied to the loop, and the current generated causes an increase in temperature. The anode, which is positive with respect to the filament, forms powerful attractive forces for electrons and this causes electrons to accelerate towards the anode to an energy that it is typically in the range of 500eV to 30keV.

The beam of the electrons leaving the gun is then collimated by one or more electromagnetic condense lenses focused by an objective lenses and scanned and focused across the specimen by scan coils. These deflection coils, inside a vacuum chamber, are energized (by varying the voltage produced by the scan generator) and create a magnetic field which deflects the beam back and forth, and therefore the samples are scanned in lines [1].
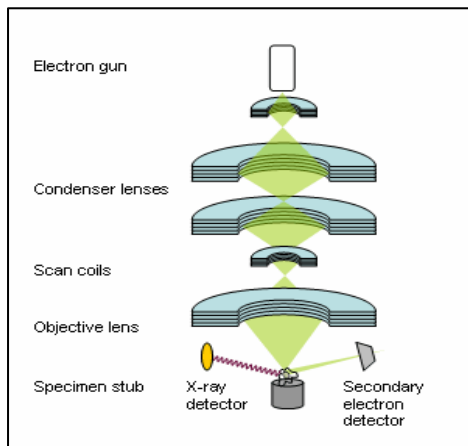
Fig 2.1 Simplified sketch of a SEM. In this sketch can different parts of a SEM be observed in a simplify way, such as the electron gun, lenses, scan coils and two interaction detectors [2].

When the beam strikes the sample, interactions occur inside these one and these collisions are detected with various instruments. The interactions that occur are the following: backscattered electrons, secondary electrons, auger electrons, X-rays, unscattered electrons, elasticity scattered electrons and inelastically scattered electrons. While all these signals are present in the SEM, not all of them are detected and used for information. The signals most commonly used are the Secondary Electrons and the Backscattered Electrons , we focus on these two:

➢ **Backscattered Electrons:** These electrons are generated because of an incident electron collides with an atom in the specimen which is nearly normal to the incident's path. The incident electron is then scattered "backwards" 180 degrees.

➢ **Secondary Electrons:** Caused by an incident electron passing "near" an atom in the specimen, near enough to impart some of its energy to a lower energy electron. This causes a slight energy loss and path change in the incident electron and the ionization of the electron in the specimen atom. This ionized electron then leaves the atom with a very small kinetic energy (5eV) and is then termed a "secondary electron". Each incident electron can produce several secondary electrons. Due to their low energy, 5eV, only secondary electrons which are very near the surface can exit the sample and be examined [3].
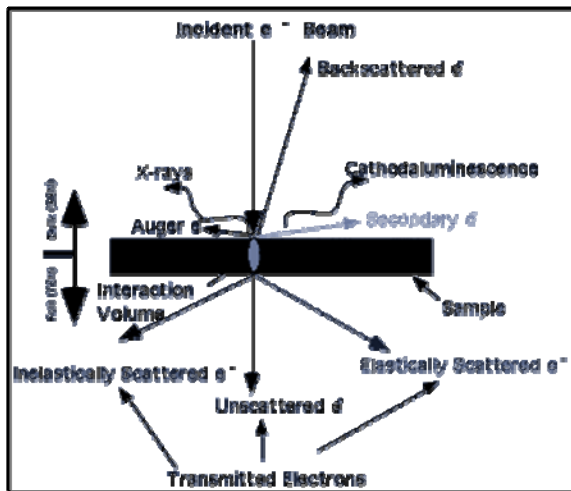
Fig 2.2 Interactions inside the sample. Sketch of all the interactions occurring inside the sample: Backscattered Electrons, Secondary Electrons, Auger Electrons, X-rays, Unscattered Electrons, Elasticity Scattered electrons and Inelastically Scattered Electrons [3].

Then the radiations from the specimen stimulated by the incident beam are detected, amplified and used to modulate the brightness of a second beam of electrons scanned, synchronously with the first beam, across the cathode ray tube display.

If the area scanned on the display tube is A x A and the corresponding area scanned on the sample is B x B, then the linear magnification is M= A/B, so this can be changed by changing the area scanned in the sample [4]. Before the beam moves to its next stay point these instruments count the number of interactions and display a pixel on a CRT whose intensity is determined by this number (the more reactions the brighter the pixel).This process is repeated until the grid scan is finished.

The SEM images presented in this thesis were accomplished by the Hitachi S-4000, with acceleration voltages of 20 kV magnifications up to 300Kx. Our samples are mounted in an aluminum sample holder using a special tape for allowing conduction, and in this way avoiding the sample charging because of the electron beam.

2.1.2 Transmission Electron Microscope

The image formation in transmission electron microscopy is essentially a diffraction phenomenon. A detail interpretation of an image requires a previous knowledge of the corresponding diffraction pattern, adequately oriented with respect to the image.
A transmission electron microscope can be schematized as three-lens systems: a condenser lenses system, an objective lenses system and a projector lenses system [4].

The electron beam then travels through the specimen you want to study. Depending on the density of the material under study, some of the electrons are scattered and disappear from the beam. At the bottom of the microscope the unscattered electrons hit a fluorescent screen, which gives rise to a "shadow image" of the specimen with its different parts displayed in varied darkness according to their density.
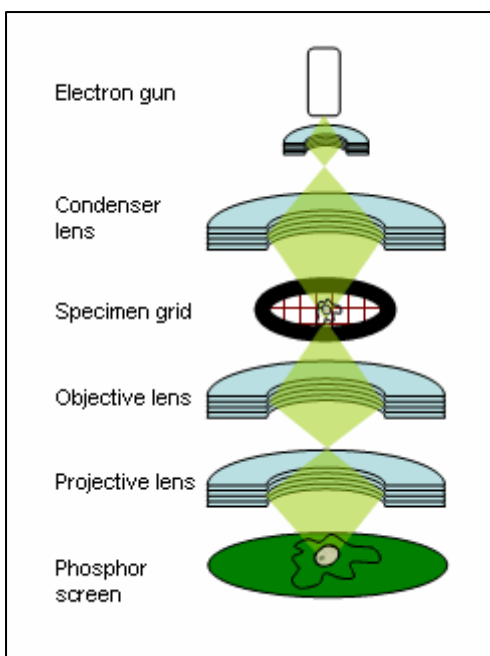
Fig 2.3 Simplified sketch of a TEM [2]. In this sketch can be observed in a simplify way different parts of a SEM, such as the electron gun, lenses, the specimen grid and the phosphorus screen

In a TEM, the specimen you want to study must be of such a low density that it allows electrons to travel through the specimen. Next it is presented a brief explanation about the sample preparation that was carried out in the application labs of Zeiss Nanotechnology in Oberkochen, during the process of TEM investigation.

Next we show the different preparation steps necessary for the TEM characterization of our samples:

(1) Surface protection
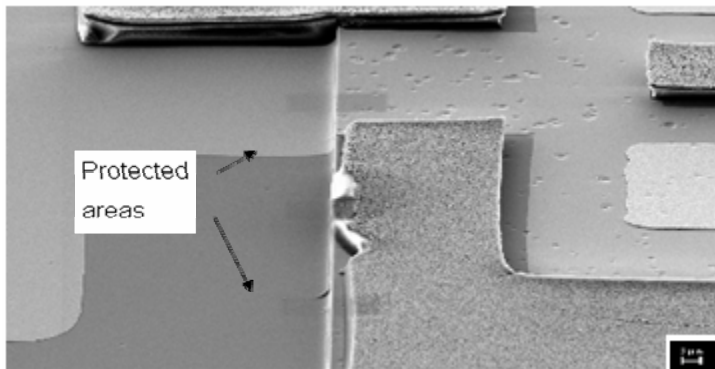
Fig 2.4 Surface protection

Firstly the surface is protected by a carbon electron beam deposition. In this process hydrocarbon is used as a precursor gas, which is cracked close to the surface and once there, is deposited.

(2) Ga-Ion milling
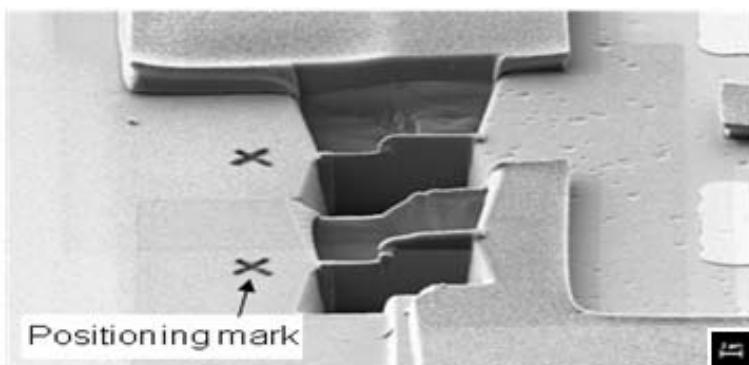
Fig 2.5 Lamella extraction

Secondly a preparation of a thin lamella (thickness ~ 200nm) is executed by removing the surrounding material. The lamella was prepared using focus ion beam (FIB) techniques.

(3) Transfer of the lamella

Fig 2.6 Lamella transfer

After creating the lamella, this thin film is glued on a manipulator and transfer to a grid holder.

(4) Thinning and polishing

Fig 2.7 Left image: Transmission through the lamella. Right image: Reflection in the lamella.

Finally a thinning and polishing procees is carried out until transmission through the lamella is possible.

2.2 Electrical measurement characterization methods
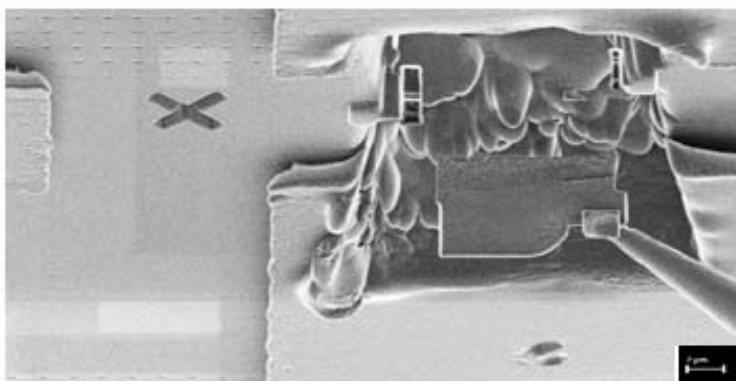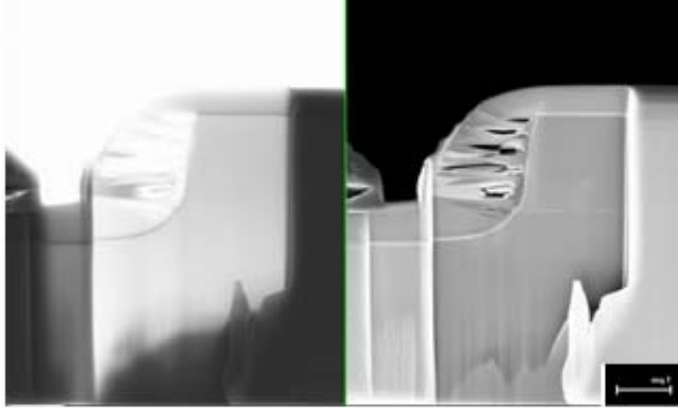
2.2.1 Operational test station

Before bonding the sample into a chip carrier, an electrical test of the nanogap electrode is performed in the operational test measurement station. In this way the successful electrodes are selected for the next step, the bonding process.

This operational test station consists of a probe station with six needles, one optical microscope and a digital source meter Keithley 2400.

With the help of the optical microscope we place two of the six available needles in the desirable place on our sample electrodes for measuring the I-V characteristics. For testing the nanogaps, one needle is placed on the top part and the other one is placed on the bottom part of the electrodes. A certain range of voltage through our electrodes is applied for checking if the nanogaps are properly working: after getting the current response of our devices and with the analysis of their I-V behavior we select the best working nanogaps.

Also the double finger structure is checked, by connecting top electrodes on the one hand, and bottom electrodes on the other hand, and with a voltage application, we test if a good connection exists between these electrodes (ohmic contact)

The testing measurements are carried out at room temperature, and normally we apply voltages from -100 mV to 100 mV for testing the nanogap behavior whereas for the double finger structure checking the range of applied voltage is between -10 mV and 10 mV. In both measurements the current compliance is set to 5µA so as to protect our samples against large current flow.

2.2.2 Low temperature measurement system

The main purpose for measuring at low temperature is because in this way we can reduce the leakage current through our semiconductor SOI structure. Next the main parts of the system will be enumerated and described:

- ➢ **Measurement tube**
- ➢ **Sample stick**
- ➢ **Sample holder**
- ➢ **T-piece**
- ➢ **Switching box**

The **measurement tube** is designed to place and measure the sample inside a liquid helium dewar. Inside the tube, vacuum and temperature conditions are maintained up to the desirable levels. It is very important to maintain a good vacuum state since in this way we avoid a possible damage of the sample when the vapor in the air is turned into ice during the cooling down process. After pumping for some minutes we reach a pressure of 1mbar, after this it is necessary to introduce a small amount of helium inside the tube through the air valve, so thermal equilibration between the inside part of the tube and the liquid helium is faster.

The **sample stick** consists of 16 cables, which form 16 independent channels with shielding up to the sample and which are connected to a switch box. The metal plates that hold the wires are connected from the bottom of the sample stick (sample holder) till the upper part of this one (T-piece) and serve additionally for reducing the airflow, getting in this way a better thermal insulation.

At the end of the sample stick the sample **holder** for the chip carrier (up to 28 pins) is situated; once the sample is placed on it, the chip carrier is in direct contact with the copper piece, being the copper a good thermal conductor. The sample copper holder is also provided with a heating resistance system. This resistance design, allows applying an extra power with the help of a temperature heater in order to be able to carry out temperature depending measurements. A calibrated Si diode temperature sensor is necessary for measuring the temperature with the help of a Model 331 Lakeshore temperature controller.


Sensor of temperature

Resistance system

28 pins for the chip carrier
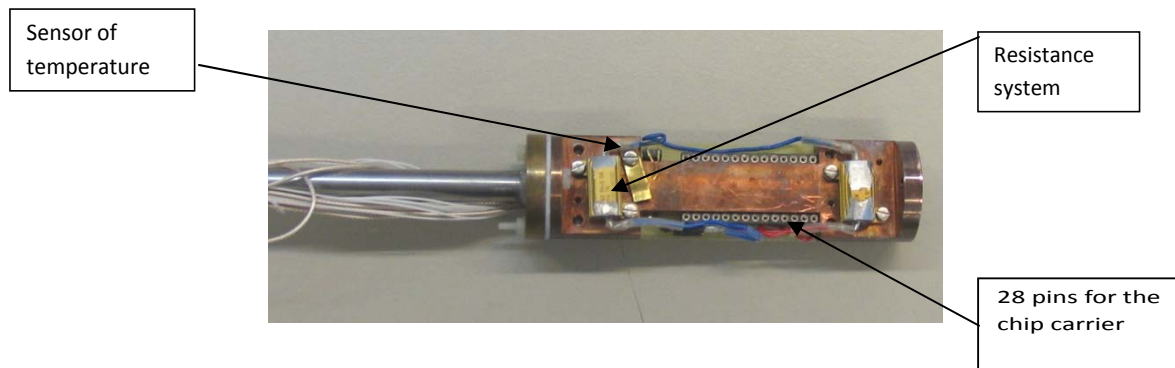
Fig. 2.8 Sample holder. In this image the resistance net, the temperature sensor and the pins for the chip carrier are shown.

The **T-piece** at the top of the sample stick, allows the connection to the temperature controller, and to the switching box, as well as contains a pressure gauge, a pressure relieve valve and an air valve.
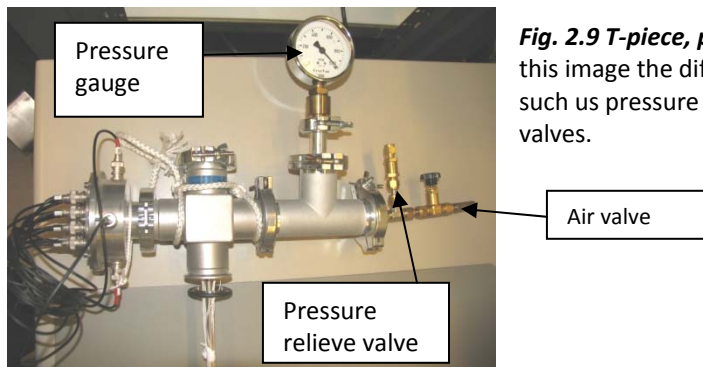
Fig. 2.9 T-piece, placed at the top of the sample-stick. In this image the different part of the T-pieces are showed, such us pressure gauge, and the pressure relieve and air valves.

The main task of the **switching box** is to allow a separate grounding of signals and shield leads. The shielding close to the sample enables low noise measurements and the grounding of the electrodes, preventing in this way a possible damaging because of electrostatic discharge. In the switching box there are 16 channels, from which the unmeasured channels are grounded for protection whereas the selected channels are switched on. Each channel can be selected separately, selecting either a common ground or a measuring exit for each one (connected to the K2400 source meter). The source meter is connected to the computer and with the help of software developed in Labview the I-V characteristics of our electrodes are recorded.
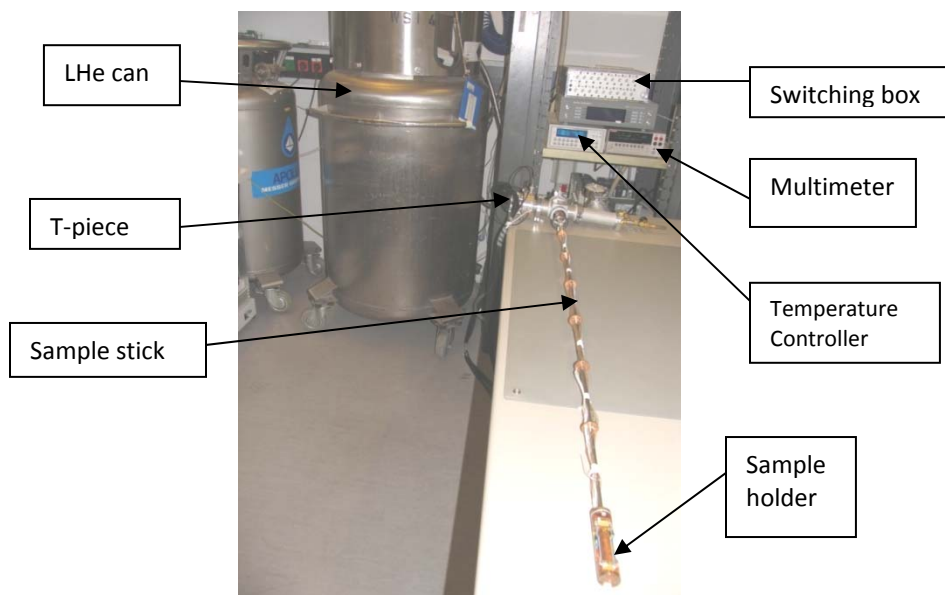
Fig. 2.10 Low temperature system measurement: In the image the set up for low temperature measurements is shown. This system consists of: LHe can, T-piece, sample stick, switching box, multimeter, temperature controller and sample holder.

2.3 Reactive ion etching (RIE)

2.3.1 General etching theory

Removing material form a substrate by a chemical or a physical method is referred to as an etch process, although we find some exception such as: scratching, grinding or polishing, since these methods are not always etching processes. An introduction about two etch mechanisms used in modern microelectronic device manufacturing is given in these paragraphs [5].

An important concept within the etching process is the anisotropy. The anisotropy of an etch process is given by the etch rates, and gives information about the rate directions in the material.

ER_L is defined as the lateral etch rate and ER_V is defined as the vertical one.

Anisotropy is given by the next equation:

$$A = 1 - \frac{ER_L}{ER_V}$$

[2.1]

- In an *Isotropic* process $ER_L = ER_V$ and A≈0 which implies that the etching rates for vertical and horizontal directions are the same.

- If an *Anisotropic* process $ER_V \gg ER_L$ and A≈1.

ISOTROPIC   **ANISOTROPIC**
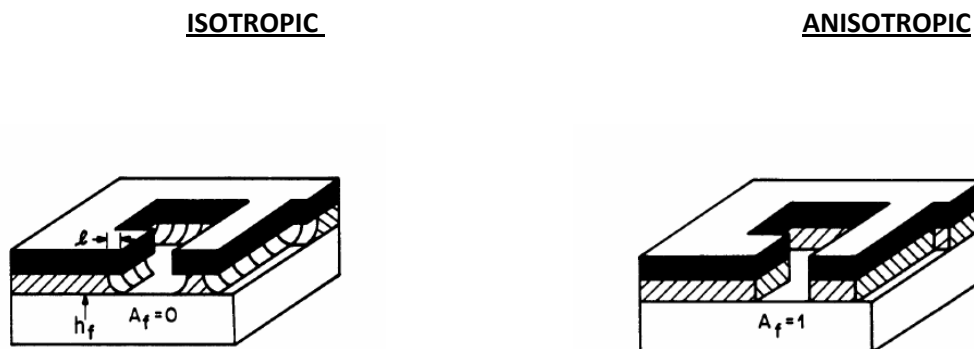
Fig 2.11 Isotropic and anisotropic process. Where if h_f is assumed to be the thickness of the thin film and l the lateral distance etched underneath the resist mask and A_f the degree of anisotropy [6].

2.3.2 Wet and dry etching

The first classification of etching processes is based on the process being either of physical or chemical nature. On the one hand the *physical etching* relies on the momentum transfer of particles hitting and eroding the surface and on the other hand the *chemical etching* relies on chemical reactions, in which some products have to be formed which are either soluble in etch solution or volatile at low pressures.

The **wet etching** is a process merely chemical which consists in three different steps:

(1) The reactive species present in a solution have to move to the surface.
(2) A reaction yielding soluble etch products has to take place.
(3) The etch products need to move away from the surface.

The wet etching is classified within isotropic etching process so undercuts below the masks are created. For the wet etching process a large number of recipes exist to etch virtually every material, high selectivity is one of the main advantages and the damage to the substrate induced by the etch process is rather low. As a clear disadvantage there is a large consumption of chemicals and handling of toxic waste.

The **dry etching** is a process where the surface is ablated by bombarding it with atoms molecules, ions or electrons. The process can be physical, chemical or a combination of both.
The two different mechanisms are encountered in dry etching are:

➢ **Sputter etching** also known as ion etching is a physical etching. A plasma (usually Argon) is ignited between two electrodes, the ions in the plasma are accelerated to the surface by an electric field. When the ions hit the surface, the energy is high enough to mechanically knock out single atoms from the surface. Any material can be etched; therefore the selectivity is low, which results in a fast ablation of the masks. In this case the etch products are not volatile and can be re-deposited on the surface, which can lead to a roughening.

➢ **Chemical dry etching** involves a chemical reaction between gas particles and atoms on the surface. The surface material is spontaneously etched from the neutral or activated gas and forms volatile etch products. Prerequisite is the formation of gaseous volatile reaction products which can be pumped out of the chamber using a vacuum pump. Since the speed of these neutral particles is generally uniformly distributed, the etching profile is generally isotropic. The selectivity is comparable higher as in a wet etching.

2.3.3 Reactive ion etching process

Reactive Ion Etching (RIE) is an etching process where a combination of mechanisms is used. It is also known as reactive sputter etching, since instead of inert gases, reactive gases such us fluorine, chlorine, bromine or oxygen are employed. The role of the accelerated ions can be either to make a low-reactive surface more reactive due to damaging or to supply additional energy for etching products to be desorbed from the surface. Ions are directed to the surface and react chemically with the material. In principle the plasma etching is a chemical etching, not a physical etching but because of the existing DC bias, there is always some sputtering.

The RIE process can be defined as a combination of a plasma tool with the use of reactive gases. Plasma etching is referred to the configuration of the reactor, and in this case the wafer is in direct contact with the plasma and all the wafer is exposed to the same pressure level. The chambers are typically compact and have low volume. In contrast to the ion beam etching (IBE) where the wafer is held at low pressure in a large chamber, then the plasma is generated in a separate ion source afterwards the ions are accelerated onto the wafer by applying appropriate voltages to a set of grids in front of the source [7].

(a) The reactive ion etching machine

The etching reactor consists basically of a vacuum chamber, an inlet for the gas and an outlet to the vacuum pump. Two parallel discoidal electrodes are located at the top and bottom of the etching chamber. The sample which should be etched is placed on the cathode at the bottom of the etching chamber. The subsequent inflow of etching gasses is electronically controlled; composition, pressure and flow are continuously regulated.
A radio RF electrical field is applied between the electrodes bringing the gas to a glow discharge. The result is a low pressure, low temperature plasma containing electrons and various species of the reaction gas such us positive or negative ions, neutral or excited molecules [8].
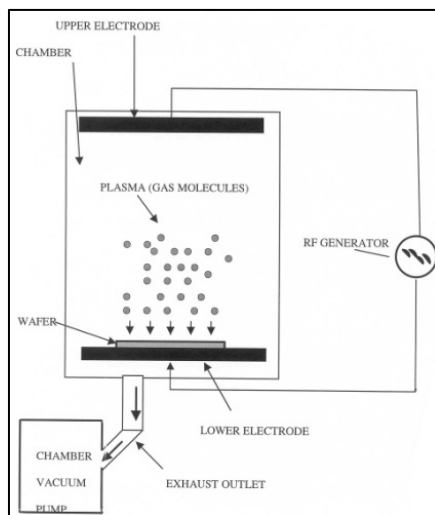
Fig 2.12 Schematic of a RIE plasma chamber. In this figure the RF generator, the RIE chamber, the electrodes, the wafer and the vacuum system are shown [9].

a.1 Plasma generation and etching mechanisms

When a high voltage is applied between two electrodes in the plasma chamber, the gas molecules are accelerated and ionized by collisions forming a plasma. A plasma is a (partially) ionized gas.

In the plasmas we deal with, free electrons collide with neutral atoms/molecules and, through a dissociative process, they can remove one electron from atom/molecule, which gives a net result of two electrons and one ion.

Depending on the energy of the incoming electron, this collision can result also in other species, such us negative ions, because of electron association, excited molecules, neutral atoms and ions.

During the etching mechanisms a chemical etching takes place: this means that a chemical reaction occurs between the solid atom (from the film to be etched) and gas atoms to form a molecule, which is removed from the substrate.

The main steps in etching process are:

1) Formation of the reactive particle
2) Arrival of the reactive particle at the surface to be etched
3) Adsorption of the reactive particle at the surface to be etched
4) Chemisorptions of the reactive particle at the surface (chemical bond is formed)
5) Formation of the product molecule
6) Desorption of the product molecule
7) Removal of the product molecule from the reactor

In our experiments for the silicon etching we will use a mixture between C_4F_8 and SF_6.
Volatile SiF_4 is formed, desorbs from the surface and is removed from the chamber by the vacuum pump.

Next, in more detail, we will go through the seven steps involved in an etching process, more concretely in the etching of silicon using SF_6.

The gases enter the reactor in form of molecules. In general these molecules are not reactive enough to react chemically with the substrate. The plasma is able to dissociate the molecules into reactive atoms (radicals).
For our example:

$e^- + SF_6 \rightarrow SF_5 + F + e^-$
$e^- + SF_5 \rightarrow SF_4 + F + e^-$
$e^- + SF_4 \rightarrow SF_3 + F + e^-$
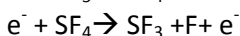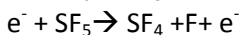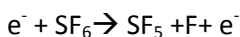
The fluorine has then to diffuse to the surface of the substrate. Only a part of formed fluorine atoms will arrive, a part will recombine, another part can be lost onto the walls or go out with the pumping.

The fluorine has then to absorb (Van der Waals bond) and then to chemisorb (covalent bond) with the silicon

$$Si + F \rightarrow SiF$$
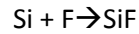
Since, SiF is not a volatile molecule, it will remain in the surface. The first volatile compound formed is SiF4. This compound can be formed by two ways:

A)

$$SiF+F \rightarrow SiF_2$$
$$SiF_2+SiF_2 \rightarrow SiF_4+Si$$

B)

$$SiF+F \rightarrow SiF_2$$
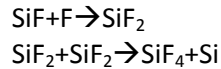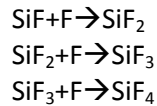$$SiF_2+F \rightarrow SiF_3$$
$$SiF_3+F \rightarrow SiF_4$$

Once SiF_4 is formed at the surface of the substrate, it can desorb form the surface and become a gas molecule, which is then removed from the reactor through the pump to the exhaust.

Fig 2.13 Detail in the plasma chamber. The plasma generated can be observed through the window.

(b) RIE chamber operation

In general the frequency of the applied power is typically 13.56 MHz, and frequencies in this range can be easily followed by electrons.

The free electrons are able to follow the variations of the applied electric field and they will consequently travel much longer distances than the ions, and they will much more frequently collide with the reactor walls and electrodes, so as a result the electrons are removed from the plasma. Therefore a negative charging of isolated electrodes is generated due to the higher mobility of the electrons.

The bulk of the plasma becomes more positive, however plasmas remain neutral. To guarantee this neutrality a DC electric field has to be formed in such a way that the electrons are repelled form the wall. Thus, it is necessary to place a capacitor between the power generator and the electrodes, helping in this way to form the DC charge.

During the first few cycles the electrons generated in the plasma escape to the electrode and charge the capacitor negatively, therefore a negative DC is generated in the electrode, which repels the electrons.

As the electrodes are charged negatively with respect to the plasma they attract positively charged ions from the plasma. This negative charging of the electrodes equilibrates in such a way that the electron and ion currents compensate each other in temporal average.

Usually the upper electrode is connected with the chamber walls and is thus larger than the target electrode which will consequently be charged to a greater extent.

The ions attracted from the plasma have a large enough kinetic energy to activate a chemical reaction. Since the pressure in the chamber is kept very low, little collision occurs.

Therefore the path of the ions is normal to the surface and the mask pattern in transferred to the surface without change, in an anisotropic way.
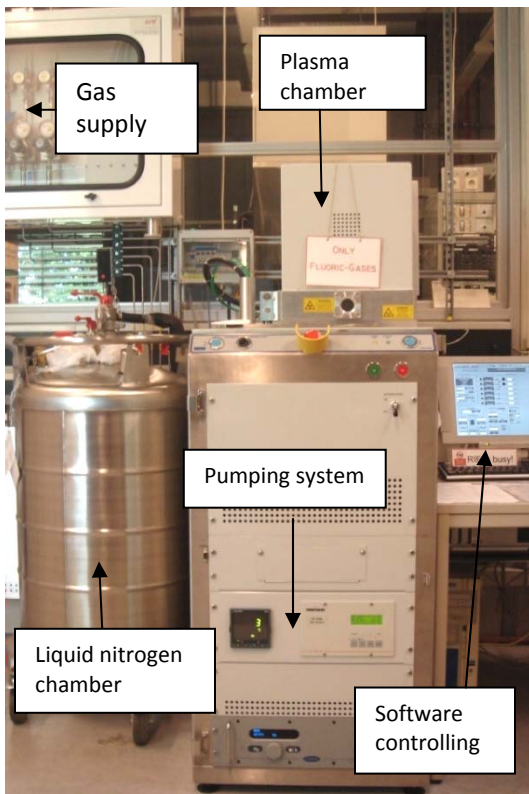
Fig. 2.14 RIE machine: The system consists of: Gas supply, liquid nitrogen dewar, plasma chamber, pumping system and software controlling.

Chapter 3

Silicon on Insulator based nanogap devices

In the first part of the chapter the nanogap fabrication process and all the steps that are involved in the manufacture of our nanoelectrodes are described. The wafer structure, the different etching steps as well as the metallic contacts deposition are explained throughout this section.

In the second part of the chapter the sample characterization is described. Both room temperature and liquid helium temperature measurements are shown in this section.

3.1 Nanogap fabrication: Steps and developing procedure

In this section the nanogap fabrication process and all the steps that are involved in the manufacture of our nanoelectrodes are described.

3.1.1 Wafer structure

The wafer structure used for our devices is SOI (Silicon on insulator), this material has been selected because of the suitable properties of the Silicon on Insulator material for further biological applications. The main advantage that SOI wafers present is that predefine our nanogap geometry by the Buried Oxide layer (BOX), in our wafers the layer width of the SiO_2 is of 20 nm. Another clear advantage is also that we can apply the standard silicon technology for the whole nanogap processing.

For the fabrication of silicon on insulator substrates standard 6" silicon wafers are oxidized, turned upside down and subsequently bonded to a second silicon wafer, which will be referred to as bulk. The silicon sitting on the insulator layer gave the name to the substrate. It is electrically separated from the bulk by the oxide which is buried underneath the SOI layer and will thus be referred to later as the BOX.

In our nanoelectrode manufacture we use the following structure:
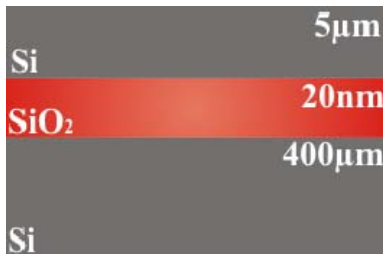
Fig 3.1 Silicon on Insulator wafer structure This sketch shows our SOI geometry: A layer of SiO_2(20 nm) is placed between two silicon layers (5µm, the upper one and 400 µm the lower one)

For the fabrication of our devices the wafers are divided into small pieces by cleaving or sawing, and processed separately as it is explained in the next sections [1]. As the wafers were covered with photoresist before the sawing process in order not to be damaged, the first step in the preparation of our devices is to clean the samples. The process for cleaning the samples consists of:

-Immersion the sample in acetone ca 10 min.
-Flashing with clean Acetone.
-Flashing with clean Isopropanol.
-Dry with a stream of Nitrogen.

The next etching steps define the pattern of our SOI structure by etching the top silicon until we reach the SiO_2, the later position of the nanogap.

3.1.2 Etching steps

In this section the several steps involved in the etching process are described, concretely the reactive ion etching steps, until we reach the SiO$_2$ layer in our SOI wafer. Once the silicon dioxide is reached, this layer is exposed to a wet etching for defining the nanogap region.

The first step towards the nanoelectrodes pattern consists on spin coating, which means the photoresist deposition for the first RIE etching.

Firstly we get rid of the humidity, after the cleaning process, in the oven at 120° for 10 minutes, and we place the sample on the spinner. Before the spin coating, we dry the sample gently with a nitrogen stream, to avoid some remaining dust in the surface. Carefully we place some drops of 1818 positive photoresist on the sample, placing it with the syringe in the middle of the sample chuck. The spinner configuration consists of a rotational speed of 6000 rpm applied for 40 seconds and resulting in a photoresist layer of ca 1.6 μm. After the first layer of photoresist we clean carefully the edges of the sample, since some excess of photoresist usually stay there after the spinning process, and this can result in a non well-leveled photoresist layer, and in this way we avoid possible problems in the lithography process.

After the edges cleaning we proceeded to make a soft bake step in the hot plate for 2 minutes at a temperature of 120° C. The second spin coating process comes next with exactly the same configuration parameters than before. The reason of putting the photoresist in two spinning coating process is to achieve a thickness of 3.2 μm of photoresist layer. After the second photoresist placement we make a soft bake of the sample, on the hotplate at 120° C for 5 minutes.

Next we make the first lithography step; a lightening during 18 seconds is necessary to transfer the mask pattern to the sample, followed by a developing step of 48 seconds in the corresponding developer solvent. For positive photoresists, the resist is exposed with UV light wherever the underlying material is to be removed. In these resists, an exposition to the UV light implies a change in their chemical structure so that it becomes more soluble in the developer. The exposed resist is then washed away by the developer solution, leaving windows with access of the bare underlying material.
We define in this way 26 structures corresponding with 26 nanogaps which are patterned by means of the following silicon technology procedures. During the following first RIE step we carry out an etching for 12 minutes and we expect to etch the most part of the first silicon layer in our SOI structure.

Fig 3.2 First RIE step This sketch shows us the application zone of the RIE1, as well the positive 1818 photoresist that is placed on the first silicon layer, after the a lithography step.

We make a chamber cleaning before starting the RIE process to be sure that he conditions are the most suitable ones, and no contamination remains in the chamber. The cleaning camber consists of two steps, in the first step for 5 minutes and at 20° C, we apply a glas-flow [sccm] of SF_6= 20 and O_2=100.In the second step for 10 minutes and at 20° C, we apply a glas-flow [sccm] of SF_6= 20 and C_4F_8=30.

The first RIE lasts 12 minutes, at 10° C, we apply a glas-flow [sccm] of SF_6= 20 and C_4F_8=35.In this step we use Fomblin, a greasy lubricant which improves the temperature conduction between our samples and the RIE chamber.

After the first RIE we make the Fomblin cleaning to get rid of this lubricant, since will not be necessary for the next steps. The cleaning Fomblin process consists of:
-Immersion the sample in acetone ca 10 min.
-Flashing with clean Acetone.
-Immersion the sample in acetone ca 10 min.
-Flashing with clean Isopropanol.
-Dry with a stream of Nitrogen.
-Cleaning with Piranha (H_2SO_4:H_2O_2=2:1=40ml+20ml) for 10 minutes.

After the Fomblin cleaning we measure the etched depth in the Dektak 3030, which is an advanced surface profile measuring system, which accurately measures vertical features in our case the etched depth.
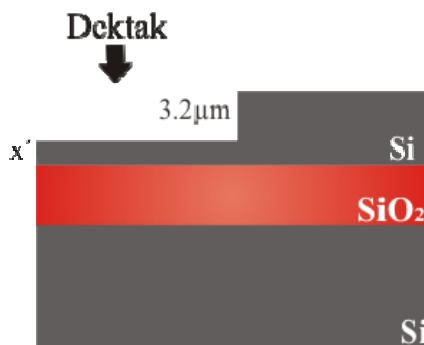
Fig 3.3 Etch depth measurement This sketch shows the lateral shape of the SOI sample after the first RIE step.
The etched depth during the RIE1 step is measured for calculating the etching rate , and in this way we are able to predict the necessary time for etching the remaining depth x´.

In general the etching rate can be calculated in this way:

$$Etching\_rate = \frac{depth\_RIE1}{time} = rate\frac{nm}{s}$$

[3.1]

In our devices we measure the depth etched during the first RIE process which is typically around 3.2 µm. In this way we can calculate the etching rate:

$$Etching\_rate = \frac{3.2\,\mu m}{12\min} = 4.4\frac{nm}{s}$$

[3.2]

For the remaining 1.8 µm we calculate an etching time of 454 seconds for the second RIE step, including a safety margin of 200 nm. After the second RIE we expect to have the next situation in our devices:
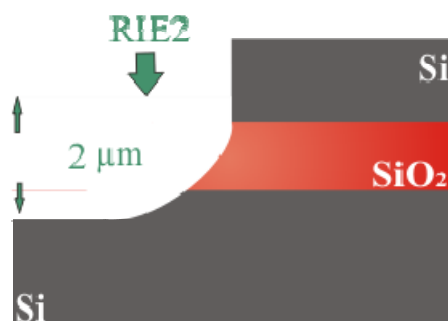
Fig 3.4 Second RIE step This sketch shows   the result after applying the RIE2.This etching rate is not so fast for the SiO_2 material that is why we obtained a rounded shape after the etching step in this oxide layer.

By means of this etching step we leave uncovered the SiO_2 BOX zone for a post-wet selective etching step. In the next step we proceed to define a trench, by means of a wet selective etching.

3.1.3 Trench definition: A selective etching process

A common wet etch process to remove Silicon dioxide (SiO_2 etching) is to use a diluted solution of hydrofluoric acid (HF), as it offers an extremely high selectivity to silicon of about 1:100.The overall reaction for etching SiO_2 is [2]:

$$SiO2 + 4HF \rightarrow SiF4 + 2H2O$$

[3.3]

We immerse the sample in a 5% concentration HF for 8 minutes and we etch the gap region in the SiO_2 layer.

Fig 3.5 Selective nanogap etching step This sketch shows the formation of a trench by the selective removing of the silicon oxide with HF.

After the immersion we make two washing steps in de-ionized water for 5 minutes, and we flash the samples gently. The samples are dried in a nitrogen stream, afterwards.

The third RIE step comes next, we carry out an etching for 30 seconds .This additional reactive ion etching step improves visibility at SEM of the planar geometry.

Fig 3.6 Third RIE step. This sketch shows us the result in the geometry of the devices after applying the RIE3, we remove the geometrical displacement between the upper and the lower electrode and a more symmetrical geometry it is achieved.

3.1.4 Metallic contacts

Once we have defined the geometry of our nanogaps devices, the metallic pads have to be applied on our structure. The steps followed are the next:

Firstly we make the spin coating as it is explained in the section 3.1.2. Next we make the first lithography step; a lightening during 5.5 seconds is necessary to transfer the mask pattern to the sample, and a developing step of 48 seconds.

The evaporation process consists on placing a layer of 100Å of titanium plus 2100Å of gold via beam evaporation. The purpose of the titanium is to make more stable the adhesion of the metallic pads on the surface.

After the metallic evaporation we carry out a lift-off. In a lifting off, after having defined a pattern on a substrate and having evaporated a metallic film all over the substrate (covering all areas, including the ones where the photoresist has been removed after the developing process), the photorresist under the film is removed with solvent (Acetone). In this way it takes the film away with it, and leaves only the film which was deposited directly on the substrate.

The result in our samples is to get double-finger metallic pads of a height of 2200 Å (220 nm)

The double finger structure implies that there are two metallic pads in the upper electrode as well as in the bottom electrode and in this way the electrical testing of the electrodes is more reliable.
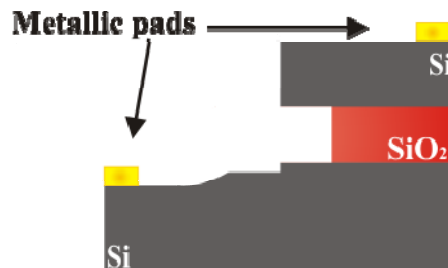
Fig 3.7 Metallic pads evaporation This sketch shows us the placement of the metallic pads for contacting the sample, after the evaporation and the lift-off process.

3.1.5 Thin layer for gold electrodes design

Once the metallic pads are patterned in our devices comes the final step: the definition of the thin layer which will connect the double finger of the electrodes, and will form the connections for the molecules placement.

The placement of the photoresist for the creation of the thin layer consists of the next steps: A spin coating of negative photoresist. The spinner configuration consists of a rotational speed of 2000 rpm applied for 30 seconds, which implies a laid photoresist layer of ca 3.8 μm. After the first layer of photoresist we clean carefully the edges of the sample and we proceed to make a soft bake step in the hot plate for 3 minutes at a temperature of 95° C.

Exposure to the UV light causes the negative resist to become polymerized, and more difficult to dissolve. Thus, the negative resist remains on the surface wherever it is exposed, and the developer solution removes only the unexposed portions. Masks used for negative photoresists, therefore, contain the inverse of the pattern to be transferred. The UV lightening in the mask aligner is equal to 0.7 seconds in which the desirable pattern will be imprinted on our device. Before making the developing step of the negative photoresist we make a step this pre-bake step consists on baking the sample in the hot-plate during 1:30 minutes at a temperature of 110 ° C. The developing is carried out during 73 seconds in the AZ 400K 1:2 developer.
The main purpose for choosing a negative photoresist is because of the lift off process is more effective with negative photoresist.

Before making the metallic thin layer evaporation we make an O_2-Plasma cleaning during 300 seconds at 200 W of power, so as to get rid of some photoresist in the nanogap region that can remain after the developing process, and avoid in this a possible damage of the nanogap properties.

The sample is placed in a holder which allows evaporation with an angle of 45° and the amount of material that we evaporate is: 10 Å of titanium and 85 Å of gold (≈10 nm). After the angular evaporation a lift-off process is executed, resulting in the final pattern of the thin layer.
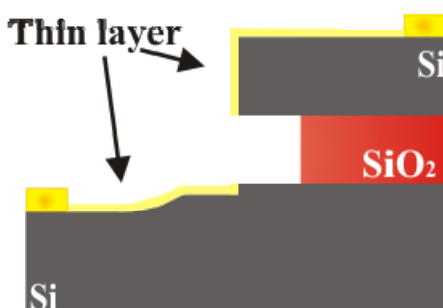

Fig 3.8 Thin layer This sketch shows us the placement of the thin layer after an angular evaporation and the subsequent lift-off process.

3.2 Characterization of finger structures

In this section the two ways of sample characterization are explained, one the one hand by means of TEM and SEM and on the other hand by using electrical techniques.

3.2.1 Sample characterization

Next, two SEM images of a sample are shown, where interesting areas of our samples, such us the metallic pads and the thin layer are marked and magnified.
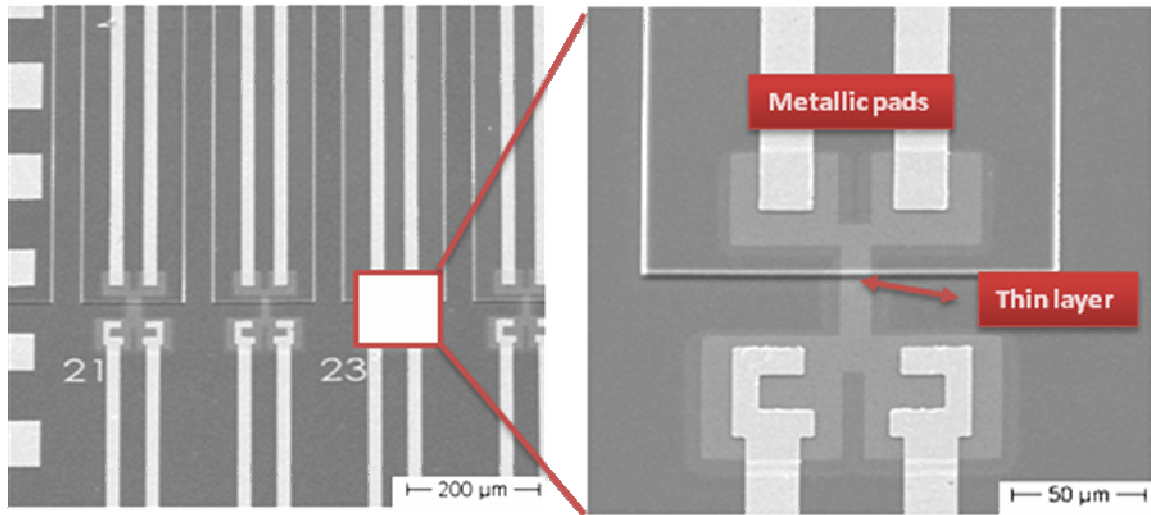
Fig 3.9 SEM images In these SEM images we can distinguish several devices performed in a sample (left image) .The right SEM image is a magnification of the nanogap nearer region, where the metallic pads and the thin layer are specified.

Hereby two TEM images are shown, where the geometry of the nanogap can be observed clearly, and also in more detail its real width of around 26 nm.
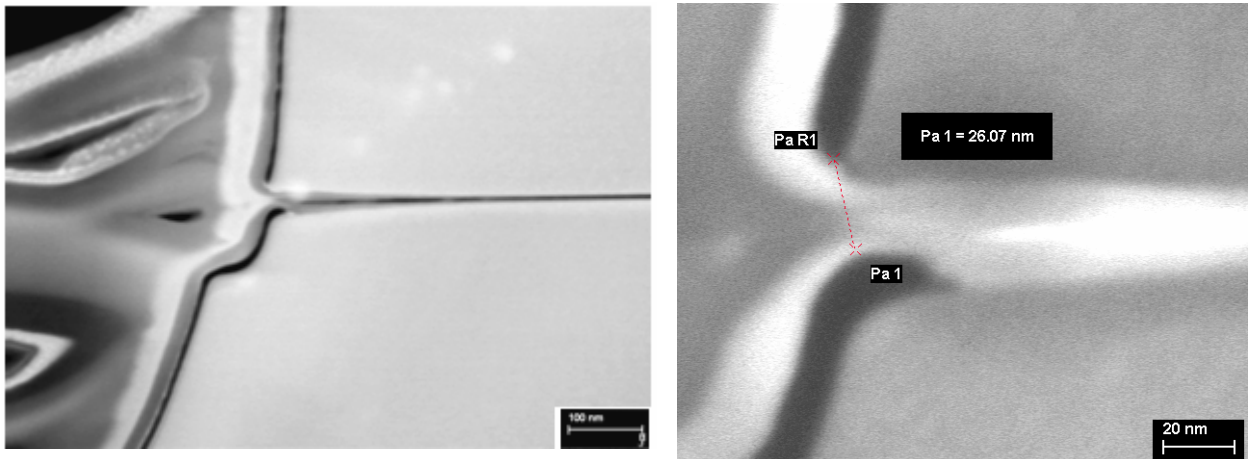

Fig 3.10 TEM images These images show the nanogap geometry. On the right image specifically we can observe the measured nanogap width which is around 26 nm.

3.2.2 Electrical characterization

The first step of the electrical characterization in our devices is carried out at room temperature, in the probe station in order to select the best working fingers, before the bonding process. The first possibility for testing the proper working electrodes, is given by the double finger measurement, which implies an electrical checking of the upper and on the lower electrodes. A good contact between the double finger both on the lower part and in the bottom part, is a strong affirmative argument for a good contact and conduction of the thin metal layer.

We expect to have an insulating behavior between the top and the bottom contacts, implying there is not short cut between the upper and the lower electrode. Next we present three different measurements demonstrating the operational test at room temperature.
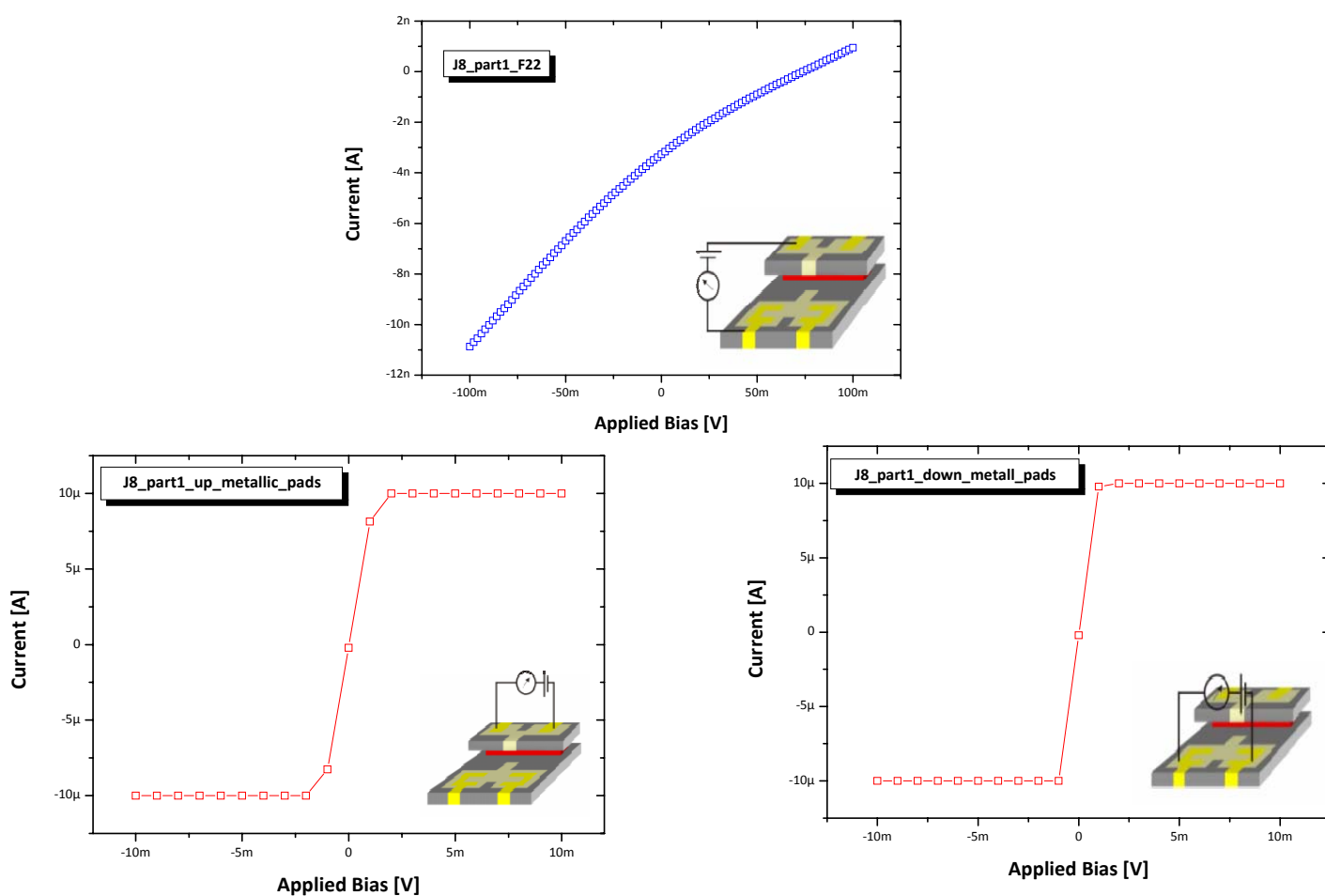
Figure 3.11 Electrode operational test at room temperature. In the upper part it is shown one typical I-V curve measured between top and bottom electrodes. In this case we attribute a nanogap resistance of 17 MΩ .In the bottom part of the figure, are shown two typical IV-curves measured between the contact pads on the same finger (up and bottom metallic pads). Working devices show a maximal resistance not larger than a few kΩ, as it is in the case for this device. To avoid a destroying of the contacts by a too high current a compliance of a 5μA is set. The insets illustrate the experimental setup.

After selecting the successful fingers we make the bonding process were the sample is placed in a chip carrier, to improve the mechanical handling. Once the sample is connected to the carrier, we can mount it in the low temperature sample tube and carry out the reference measurements at liquid helium temperature (See low temperature measurements chapter 2)

Next we observe in the figure 3.12, one typical I-V curve measured between top and bottom contacts of our nanogap, at Liquid Helium (LHe) temperature (4.2 K). The resistance of the fingers increase, with respect to the values obtained at room temperature, due to the suppression of leakage current through the semiconductor structure. The resistance values for the nanogaps are larger than 10 GΩ, in this case we find a resistance of 52 GΩ.
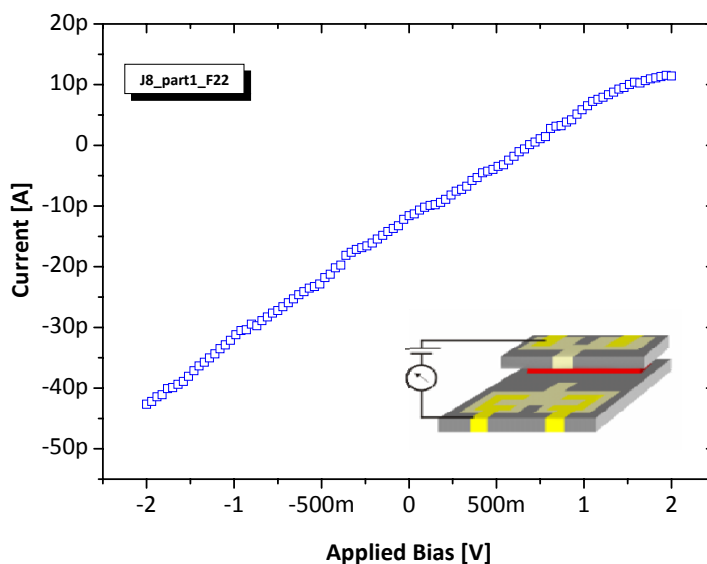
Figure 3.12 Electrode operational test at LHe temperature. In this graphic the typical I-V curve measured between top and bottom contact of the electrode at LHe temperature is shown and in this case we attribute a resistance of 52 GΩ to the nanogap. The inset illustrates the experimental setup for the nanogap measurement.

Also at LHe temperature the connections of the upper and the lower electrodes are checked, and the same behavior as the one at room temperature is obtained, showing also a maximal resistance not bigger than a few kΩ.

Chapter 4

_____

Metallic nanoparticles positioning

In the first part of the chapter a theoretical review is developed, concepts like a self assembled monolayer and forces involved in the metallic nanoparticle trapping are explained.

In the second part of the chapter the experimental process for achieving a two- junction system is described: firstly the self assembled monolayer building and secondly the gold nanoparticle positioning.

4.1 Theoretical key concepts review

In this section we give an overview of the most important theoretical concepts which are involved in our experiments.

4.1.1 Self Assembled Monolayer

Self-assembled monolayers (SAMs) are ordered molecular assemblies which form spontaneously by the adsorption of a surfactant with a specific affinity of its headgroup to a substrate. These monolayers provide a convenient, flexible, and simple system to tailor the interfacial properties of metals, metal oxides, and semiconductors.

The adsorption energy is the strongest of all interactions inside our system and presumably the primary driving force for the self-assembly process, within adsorption, two concepts such as chemisorption and physisorption need to be distinguished.

On the one hand the *chemisorption* is defined as the type of adsorption whereby a molecule adheres to a surface through the formation of a chemical bond whereas the *physisorption* is the kind of adsorption in which the adsorbate adheres to the surface only by weak intermolecular interactions (Van der Waals forces).

The most extensively studied class of SAMs is derived from the adsorption of alkanethiols on surfaces of noble and coinage metals. In this case, it is possible to generate well-defined organic surfaces with useful and highly alterable chemical functionalities displayed at the exposed interface [1, 2].

In the following Figure 4.1 a sketch of a SAM structure is shown:
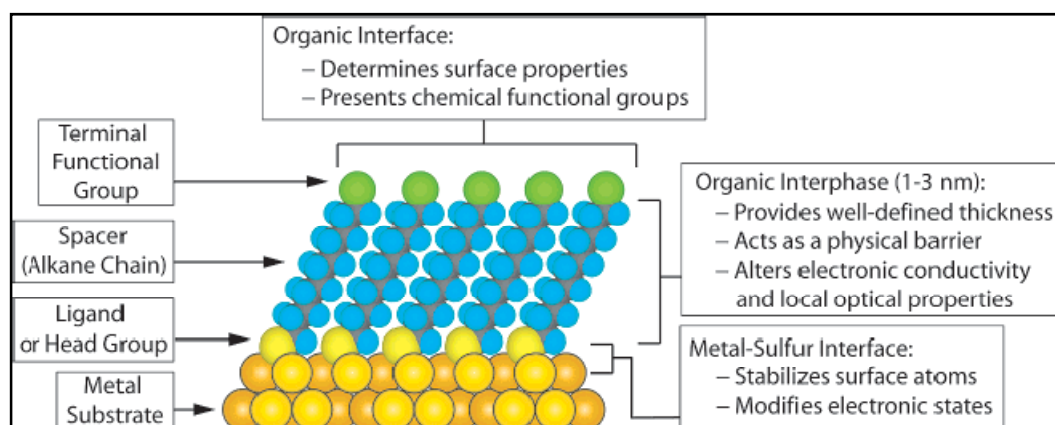
Fig 4.1 Schematic diagram of an ideal, single-crystalline SAM of alkanethiolates supported on a gold surface with a (111) texture. The anatomy of the SAM is highlighted [1].

4.1.2 Metal nanoparticle assembly forces

In this section we make a study about the direct assembly of nanoparticles in the nanogap region and the forces which are involved in this process.

Once the electrical dipole moment is created, the primary forces acting on a nanoparticle are:

- Dielectrophoresis effect
- Electrophoresis
- Electrostatic repulsion
- Diffusion

Next the most important forces in the context of my work are explained.

• **Electrical dipole moment**

If the electrical properties of a polarisable particle (i.e. its electrical conductivity and dielectric constant) differ from those of the suspending medium, an applied electric field induces a dipole moment in the particle. This is depicted in figure 4.2. The Debye is a unit of electrical dipole moment, in SI units; 1 D equals $3.33564*10^{-30}$ coulomb meter.
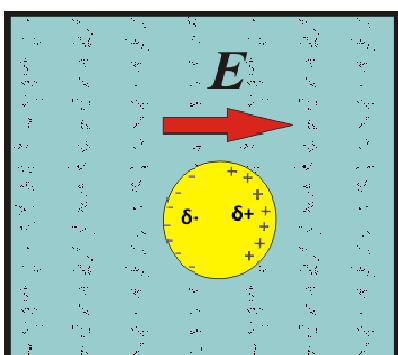
Fig 4.2 Dipole moment formation . In this sketch it is shown how an applied electric field induces a dipole moment in a polarisable particle.

Thus, for the situation shown in Figure 4.3 the induced dipole moment arising from the two induced charges + and - located at r^- and r^+ respectively, is given by equation 4.1:

$$m = (\delta_+)r_+ - (\delta_-)r_- = \delta q.r$$

[4.1]

where r is the particle radius. The dipole moments associated with interfacial polarizations can exert their influence up to frequencies of 50 MHz and beyond, this means that the particle can be polarized up to this limit [3].

- ## **Dielectrophoresis effect**

Taken together magnitude, polarity and time response of the dipole moment induced in a particle when it is under the effect of an electric field, appears the concept of dielectrophoresis. The dielectrophoresis effect is defined as the force felt by a polarisable object as a result of polarization when it is placed in a non uniform electric field, therefore by using AC fields it is possible to selectively manipulate nanoparticles. For a spherical particle of radius *r*, suspended in a medium of absolute dielectric permittivity ε_s, it can be shown that the magnitude of the **dipole moment** arising from the induced interfacial charges is given by equation 4.2 [3]:

$$m = 4\pi\varepsilon_s \left(\frac{\sigma_p^* - \sigma_s^*}{\sigma_p^* + \sigma_s^*} \right) r^3 E$$

[4.2]

where σ_p^* and σ_s^* are the *complex* conductivities of the particle and of the surrounding medium. These *complex* conductivities take into account the fact that the particle and suspending medium exhibit both conduction (energy loss) and dielectric (field energy storing) properties when exposed to electrical fields, and have the mathematical form:

$$\sigma^* = \sigma + jw\varepsilon$$

[4.3]

where $w = 2\pi f$ is the angular frequency of the applied field. The dipole moment (Equation 4.2) reveals that the magnitude and polarity of the induced dipole moment depends on the frequency of the applied field and on the relative values of the conductivity and permittivity of the particle and surrounding medium.
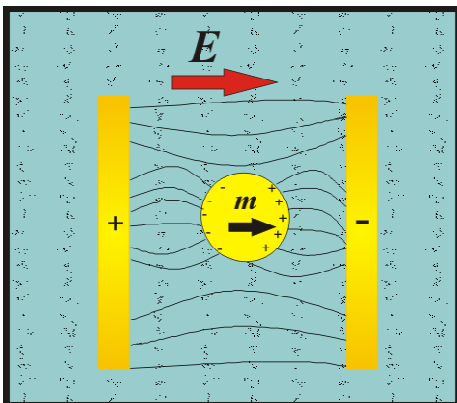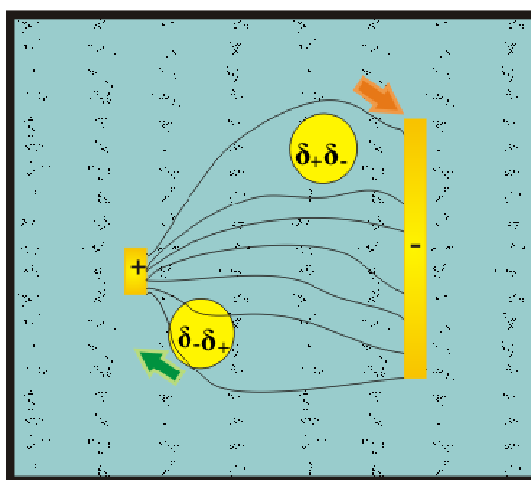

Fig 4.3 Schematic of a uniform electric field exerted to a polarisable particle. If the polarizability of the particle exceeds the one of the surrounding medium $\left(\left| \sigma_p \right| > \left| \sigma_s \right| \right)$ the arrangement of the induced charges produces a dipole moment directed with the applied field.
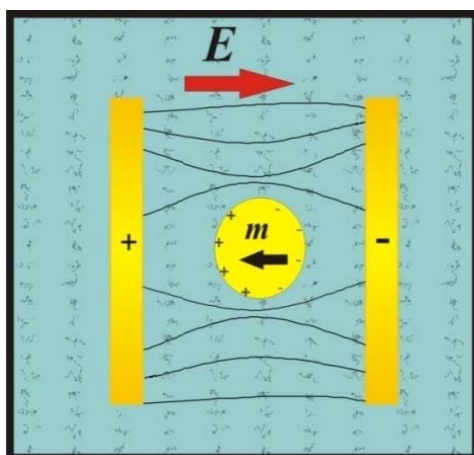
Fig 4.4 Schematic of a uniform electric field exerted in a polarisable particle. If the polarisability of the surrounding medium exceeds from the one of the particle $\left(\left|\sigma_s\right| > \left|\sigma_p\right|\right)$ the arrangement of the induced charges produces a dipole moment the moment is directed against the field.

The electric fields are generated using parallel plate electrodes, so that in the absence of the particles the fields would be uniform (neglecting fringing effects at the ends of the plates) therefore and because of the symmetry of the system *no net electrical force is exerted on the particle.* When particles are subjected to a non-uniform field an *electrical force is exerted on the particle.* This effect can be observed in the next figure where two different particles are affected by a non-uniform electric field. The particle on the left side, is more polarisable than the surrounding medium and is attracted towards the strong field at the pin electrode, whereas the particle on the right side has low polarisability and is directed away from the strong field region.

Fig 4.5 Non-uniform field effect on the particles. Schematic of a non-uniform electric field exerted in a more polarisable particle than the medium (left particle, with green arrow movement direction) and in a less polarisable particle than the medium (right particle, with orange arrow movement direction)

The total electric force acting on a particle of net charge Q in a non-uniform field *E* is:

$$F = QE + \delta q E(r_+) - \delta q E(r_-) = QE + (m\nabla)E$$

[4.4]

If the particle is uncharged (Q = 0) or for high frequencies where electrophoresis effects are negligible, the term on the right-hand side of equation 4.4, involving the dipole moment is dominating. To distinguish this force from electrophoresis the effect was termed *dielectrophoresis.*

To summarize, when a polarisable particle is placed into an electric field in vacuum or in solution, a polarization charge is induced at the surface of the object. If the applied electric field is *non uniform*, it interacts with this polarization charge to attract the object towards or against the point of strongest field.

> ➢ In the case of a particle with a larger polarizability than the surrounding medium, the interaction with a non uniform field implies an attraction of the object towards the region of highest field (positive DEP).

> ➢ In the case of a particle with a lower polarizability than the medium, the polarization charge aligns in a way that the object is pushed away from the region of highest field (negative DEP).

For a spherical particle of radius *r*, in media ε_s of permittivity, acted upon by applied field E_0, the dipole component of the DEP force is given by [4]:

$$F_{DEP} = 2\pi\varepsilon_s r^3 \, \mathrm{Re}\left\{CM(w)\nabla E_0^2(r,w)\right\}$$
[4.5]

Where *CM* denotes the Clausius-Mossotti factor, in which its real part is the determining factor for the dielectrophoretic force on a particle [4] :

$$CM(w) = \frac{\varepsilon_p - \varepsilon_s}{\varepsilon_p + 2\varepsilon_s}$$
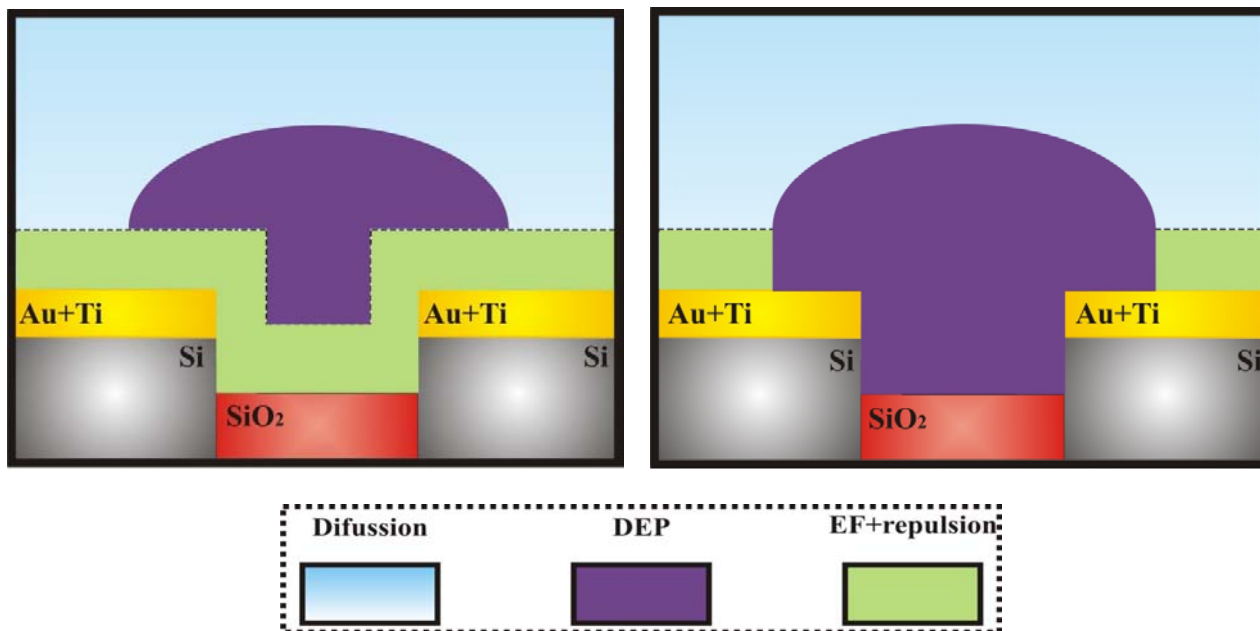[4.6]

In our experiments:

$\varepsilon_p \approx \infty$ due to the assumption of a perfectly conductive gold nanocolloid $\left(\sigma_p \rightarrow \infty\right)$. This

implies that $\mathrm{Re}\left\{CM(w)\right\}$ is calculated to be approximately = 1 and obviously

$\mathrm{Re}\left\{CM(w)\right\}$ >0, hence we are in the case of a particle under a positive DEP [5].

In the next Figure 4.6 we have represented all the forces which take part in the process of metal nanoparticle assembly:

Fig 4.6 Forces regions in the nanopaticles assembly In the left sketch we observe how the DEP cannot overwhelm diffusion and electrostatic force since the voltage is not high enough, and therefore no trapping of gold nanoparticles, inside the nanogap takes place. If the voltage is high enough, as we can observe in the right sketch, the DEP defeats both diffusion and electrostatic (EF+ repulsion) forces and therefore the dielectrophoresis is dominant in the nanogap region and the nanoparticle assembly is executed [4].

These forces have different special dependencies. The electrostatic force is typically confined to within ≈10 nm from the substrate, the diffusion force is independent regarding the nanogap region, and DEP force normally extends ≈100 nm from the nanogap.

To understand better how dielectrophoresis is involved in the nanoparticle trapping, the electric field distribution in the electrode geometry was simulated using the FEMLAB™.

As we have already explained the dielectrophoresis force is given by the following expression:

$$F_{DEP} = 2\pi\varepsilon_s r^3 \, \mathrm{Re}\left\{CM(w)\nabla E_0^2(r,w)\right\}$$ [4.7]

The subdomains were two conducting electrodes ($\varepsilon \approx \infty$) and an aqueous dielectric medium ($\varepsilon \approx 80$). The boundary conditions were:

➢ An applied voltage to the left metal electrode of 2V, positive half-cycle of the AC field.
➢ The right electrode connected to ground.
➢ The remaining boundary conditions are configured as electrically isolated.

Next the simulations from the electrostatic calculations in the nanogap electrodes (2D) are presented in the following figures:
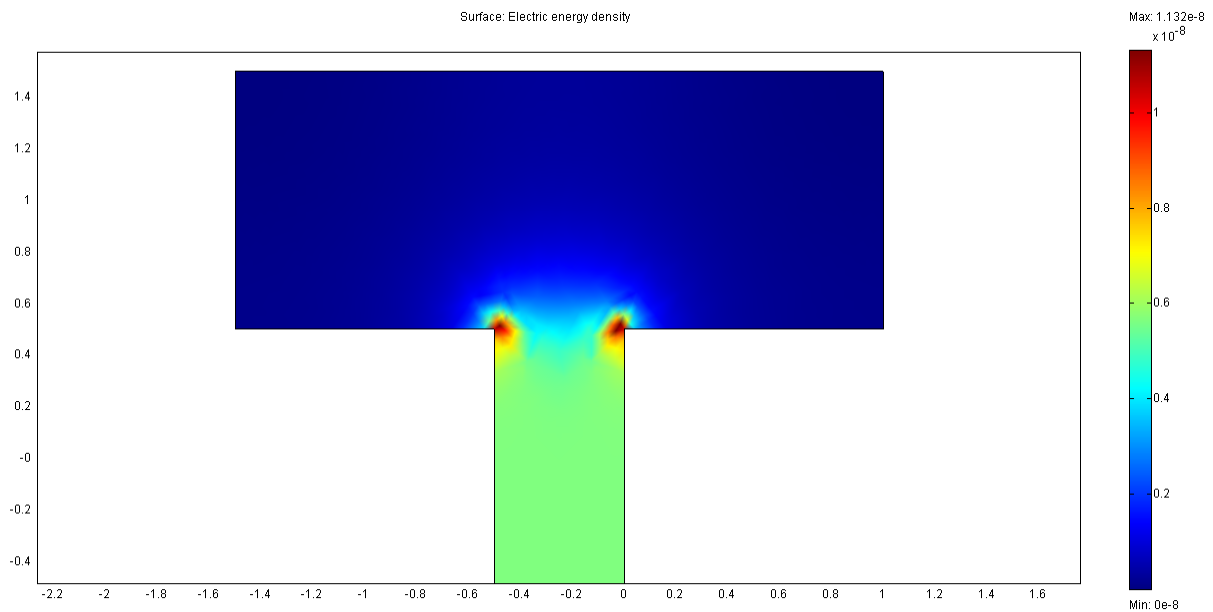

Fig 4.7 Electric energy density. In this image the electric energy density in the nanogap region is represented. In the dielectrophoretic force, this term is given by the factor: $E_0^2(r,w)$, we can observe the highest level is reached at the edges and corners of the nanoelectrodes.
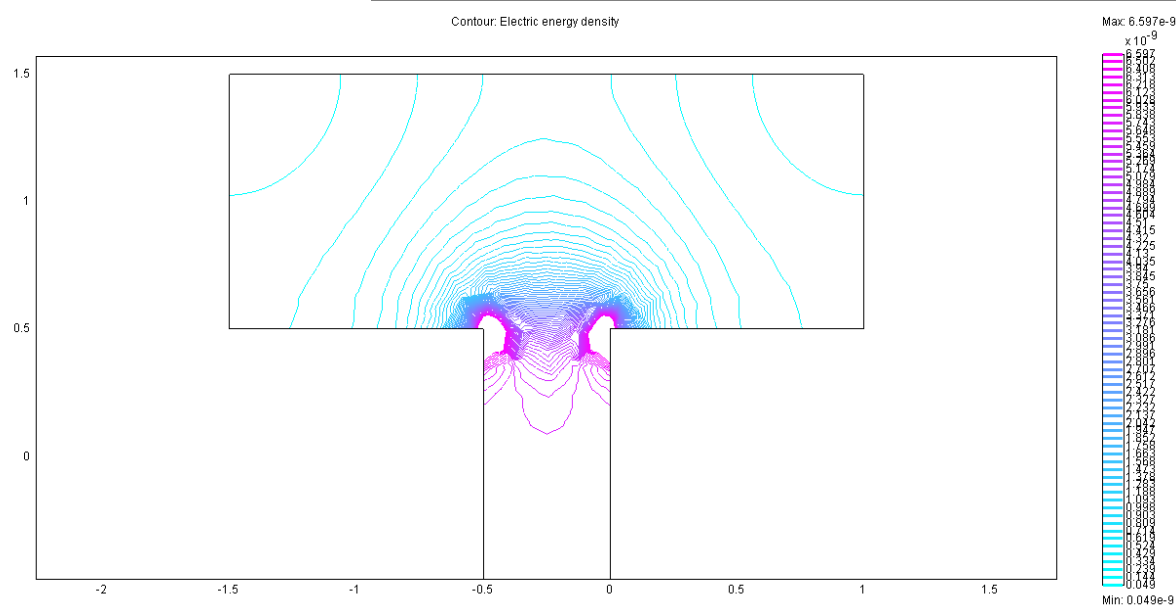
Fig 4.8 Contour of electric energy density. In this image the electric energy density is depicted as a contour, the gradient of this magnitude ($\nabla E_0^2(r, w)$) is always perpendicular to the contour lines and therefore will determine the direction of the dielectrophoretic force applied in our metallic nanoparticles. In our case this direction is towards the nanogap region since we are in positive DEP case.

As we can see in the next simulation, figure 4.9, the lines of electric field are oriented from the electrode with highest potential towards the grounded one.
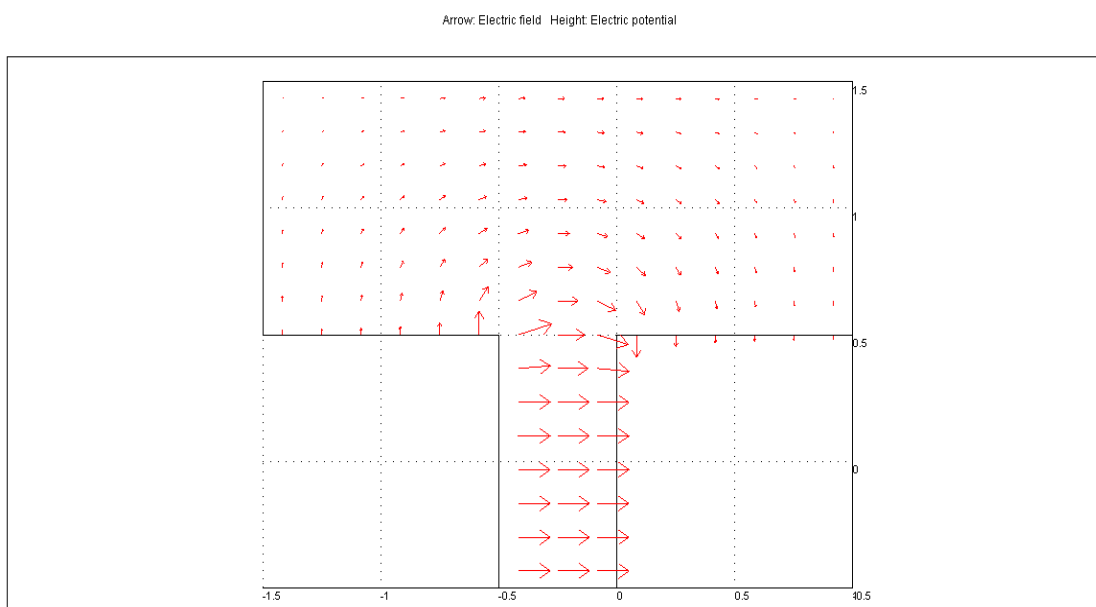
Fig 4.9 Simulation of electric field. In this image, the arrows indicate the direction of the electric field and their length represents the field strength.

• Electrophoresis force (EP)

This force is defined as the migration of charged particles through a solution under the influence of an applied electric field and it is also called *cataphoresis*. The observed lateral movement of the particle most likely results from the fact that it carries a net electrical charge Q on its surface .When it is exposed to an electric field E, a charged particle experiences a force F (*F=QE*) and the resulting motion is known as *electrophoresis.*
This movement is due to the Coulomb force, which may be related to fundamental electrical properties of the body under study and the ambient electrical conditions.

The existing electrophoresis force on the nanoparticle is described by the equation 4.8:

$$F_{EP} = \mu_{EP} C_D E$$

[4.8]

Where *E* is the electric field, μ_{EP} denotes the electrophoresis mobility which depends on both the particle properties and solution properties and it is defined as the charge between the frictional coefficient (q/f), C_D denotes the drag coefficient, which is a dimensionless quantity that describes a characteristic amount of aerodynamic drag caused by fluid flow. The drag force on any object is approximately proportional to the square of its velocity through the fluid.

The electrophoresis force depends on the polarity of the field and because of the particle's inertia the electrophoresis effect becomes vanishingly small for high frequencies. It has been studied that for length scales in the order of 10 nm there are oscillations of the particles in frequencies as high as 1MHz. These oscillations can affect the assembly process by inducing fluid flow in the surrounding medium [4].

• Electrostatic repulsion

The negatively charged nanocolloids are electrostatically repulsed by the negative charged substrate when they are less than a few Debye lengths away. The Debye length is defined as:

$$\lambda_D \equiv \sqrt{\frac{kT_e}{4\pi e^2 n_e}}$$

[4.9]

Where *k* is the Boltzmann constant, T_e is the electron temperature, *e* is the charge of the electron and n_e is the number density of electrons.

Due to the studies carried out by *Barsotti* [4], it is demonstrated that the electrostatic repulsion plays a significant role for particles within a few tens of nanometers to the substrate.

As a conclusion we extract that EP and the electrostatic repulsion (electrostatic forces), are two effects which can block the nanoparticle assembly in cases where the applied voltage is not sufficiently high for the DEP to overcome them.

4.2 Two-junction system: Au/MCH/colloid/MCH/Au system

Our two-junction system consists of two Au electrodes, on which a molecule layer has been deposited by means of a SAM process. After coating the electrodes with organic molecules an electrical trapping is developed, and as a result we achieve the positioning of gold colloids in between both molecules layers. The several steps followed in order to success in the formation of our two-junction system, is described in detail below.

In our experiments organic self-assembled monolayers (SAMs) play the role of tunnel barriers and therefore single junctions are created, where a tunneling effect exist through these layers.

4.2.1 Self Assembled Monolayer preparation

A) 6-Mercapto-1-hexanol

In our system *6-Mercapto-1-hexano* (MCH) is used as a molecule to form the functional monolayer on the gold substrate. The features of the molecules are the following:

$$SHCH_2(CH_2)_4CH_2OH$$

Fig 4.10 Sketch and chemical formula of a MCH molecule

The main interesting data of MCH molecule are:

- **Molecular formula**: 6-Mercapto-1-hexano (MCH)
- **Density** = 0.981 g/mL at 25 °C (lit.)
- **Head group**: SH
- **Spacer**: $CH_2(CH_2)_4CH_2$

The thiol group (-SH-) prefers to form a covalent bond to a gold atom of the electrodes, originating from the high affinity between these two elements a chemisorption takes place and the headgroup of the MCH molecule binds covalently to the gold surface of the electrodes.

The process of molecule assembly consists on placing 200 μl of a 1mM MCH solution onto the Au substrate, which was previously cleaned with de-ionized water.

To avoid water evaporation and light molecule damaging, the sample is locked in a beaker and wrapped with aluminum foil. After waiting 60 minutes, a SAM has built up, and the substrate is rinsed with de-ionized water to get rid of the physisorbed molecules and dried in open air for 30 minutes. The ellipsometry measurements of pure MCH layers typically show a thickness range between 0.4 and 0.7 nm, although we assume for our further calculations a molecular layer of 1nm.

Next two electrical measurements on one electrode are shown, carried out at the temperature of liquid helium (LHe), before and after the MCH assembly process. In this way we obtain an evidence of no change in the electrical characteristics of our nanogaps due to the SAM process.
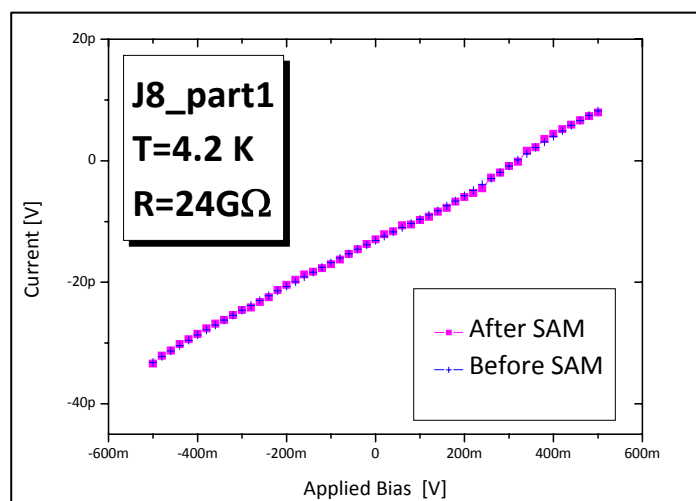
Fig 4.11 I-V characteristic before and after SAM proccess.The resitance calculated at LHe temperature for our nanogap device is in the range of GΩ, in this experiment concretely 24 GΩ.The offset that we observe in the I-V curve is originated from the measurement instrument.

B) Oligophenylenevinylene (OPV)

Another kind of molecules where also used during SAM experiments, concretely OPV_3 and OPV_7.
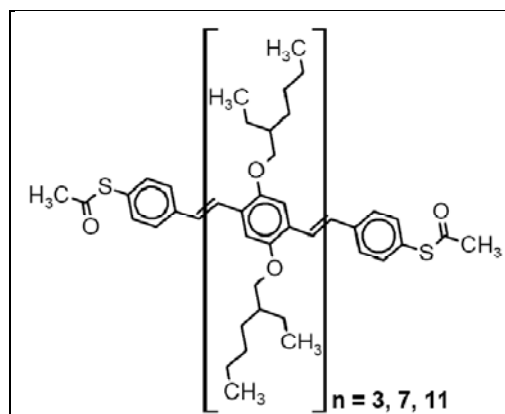
*Fig 4.12 OPV molecule sketch.*The "n" represents the number of reperating PV monomers with side chains constituing the inner part of the molecule, thereby determing its total contour length. If n=3 the molecule length is ≈3.3 nm, if n=7 the length og the molecule is ≈5.9 nm and for n=11 the length is ≈8.5 nm.

The process followed for creating an OPV SAM has the following steps:

1-Cleaning of substrate:

We immerse the carrier with the substrate in dichloromethane (DCM) for 30-60 seconds and after this we repeat the process another 3 times with DCM and 2 times with Isopropanol (IP). If it is necessary we blow the sample dry gently.
The solvent THF instead of DCM can be also used as a solvent for the molecules.

2-Soaking substrate:

We immerse the substrate in a beaker with flat glass bottom after this we add some THF to the beaker to maintain a high THF vapor pressure.
The transfer of the OPV solution is made with a glass pipette directly to the previously cleaned substrate. We use a solution of: 1.3 mg of the desirable molecule (OVP_X) and 1.7 ml of solvent (1ml THF + 0.7 ml of IP)
After the molecules deposition we cover the substrate by a clean glass slide and we put the lid on the beaker. We wrap the beaker with aluminum foil so as to avoid light damage.
Finally we wait around 18 hours for high coverage of the substrate with the molecules.

3-Washing of substrate:

We immerse the carrier with the functionalized substrate in dichloromethane (DCM) for 30-60 sec. We repeat another 3 times with DCM and 2 times with IP. And after this we wait till the sample is dried in open air.

4.2.2 Gold nanoparticles positioning experiments

In this section different scenarios are discussed whose objective is to get a suitable positioning of the metallic nanocolloids in the nanogaps.

The nanometre sized gold colloids supplied by BBInternational Company, which are used in our experiments, are characterized as follows:

- The gold nanoparticles are supplied in water, having the solution trace amounts of citrate, tannic acid and potassium carbonate.
- Citrate stabilized with a net negative surface charge.
- The 20nm gold colloids are supplied at a pH 6.0 [7].

The different kinds of gold colloids which were used during the trapping experiments are the following:

DIAMETER	AU particles per ml
20 nm	7×10^{11}
30 nm	2×10^{11}
60 nm	2.6×10^{10}

Table 4.1 Gold nanocolloids data. Diameter of gold nanocolloids with their respective denstity in solution[7].

Due to the density of the gold particles, two kind of gold suspension are used:

- **_20 nm diameter_**: 80 µl of gold colloids + 80 µl of H_2O =160 µl sol.
  $$(3.5 \times 10^{11} \text{ Gold particles per ml})$$

- **_30nm diameter_**: 80 µl of gold colloids + 80 µl of H_2O =160 µl sol.
  $$(1 \times 10^{11} \text{ Gold particles per ml})$$
  $$20 \text{ µl of gold colloids } (2 \times 10^{11} \text{Gold particles per ml})$$

- **_60nm diameter:_** 20 µl of gold colloids$(2.6 \times 10^{10}$Gold particles per ml)

We place an 8µl droplet of the gold suspension onto the electrode surface, which is previously covered with MCH or with OPV_X molecules. Once the gold deposition experiment is carried out, the samples are dipped in de-ionized water for 60 seconds and afterwards rinsed twice thoroughly for 30 seconds. The samples are finally dried carefully in a stream of nitrogen gas.
We divide our experiments in two groups: the first group where no electrical force is applied called **Gold colloids decoration experiments group**. The second experiments group: **Electrical trapping experiments group** is based on the dielectrophoresis force exertion.

A) Gold colloids decoration experiments

In our experiments a droplet of the chosen gold solution was applied in the nanogap region using a micro pipette. Two methods were followed for the nanometallic particles decoration

(1) Receding Meniscus Method

(2) Diffusion Method

(1) Receding Meniscus Method

The main idea of this method is based on the capillary force. If we wait enough time till the water evaporates the capillary exerted force pulls the particles along the surface until they are physically trapped in the nanogap region. Capillary motion is the ability of a substance to draw another substance into it. It occurs when the adhesive intermolecular forces (F_a) between the liquid and a substance are stronger than the cohesive intermolecular forces inside the liquid (F_c). The effect causes a concave meniscus to form where the substance is touching a vertical surface. [5, 6].

Fig 4.13 *Receding meniscus effect* In the left sketch it is shown how the forces are exerted in two gold nanocolloids. In the right sketch the resultant forces can be observed. When the molecules are far away from the wall, the resultant forces due to the weight and to the cohesion forces are vertical (the adhesion forces in this case are negligible), therefore the surface will be horizontal instead of vertical [6]

After a deposition of 20 nm solution (1:1) and water evaporation with subsequent water rinsing the 20 nm gold particles can be observed in the SEM image (Fig 4.14).
In the next SEM images we can observe the meniscus effect after the solution which contains the gold colloids has been evaporated.
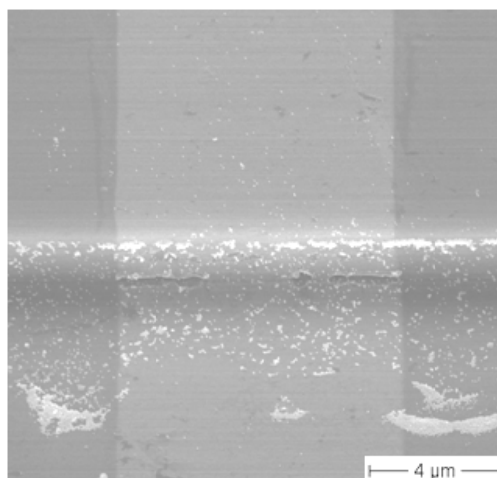
Fig 4.14 SEM image where we observe gold nanoparticles in our electrodes region, due the meniscus effect after the solvent evaporation.

Unfortunately the results obtained in the electrical measurements show that this process is not suitable for positioning of gold nanoparticles in the nanogap, since the I-V characteristics kept unaffected after the experiment and no change was observed.

(2) Diffusion method

In this case we dipped the sample in the gold nanoparticle solution and wait for 24 hours.
 Afterwards the sample was rinsed thoroughly with de-ionized water twice during 60 seconds in order to avoid salt agglomerations. It is expected that due to the Van der Waals forces some of the nanoparticles are trapped in the nanogap region

In chemistry Van der Waals forces are a sometimes used as a synonym for non-covalent or intermolecular forces, forces that are weak compared to those appearing in covalent bonding These forces are defined as a weak attractive force between atoms or nonpolar molecules caused by a temporary change in dipole moment arising from a brief shift of orbital electrons to one side of one atom or molecule, creating a similar shift in adjacent atoms or molecules

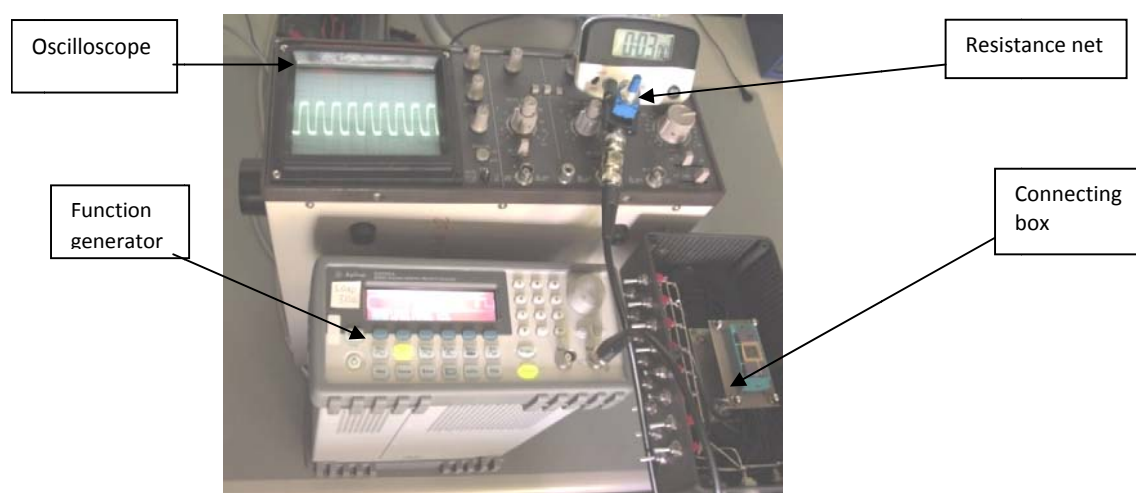The sample which took part in the experiment was analysed in the SEM and is shown in figure 4.15:
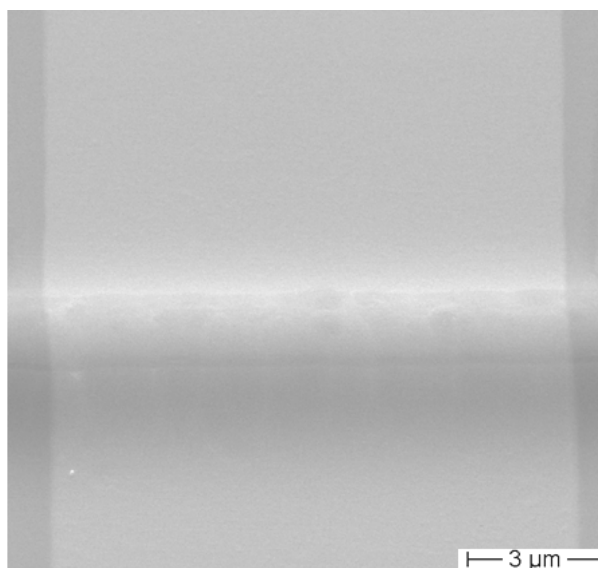
Fig 4.15 SEM image where we observe no gold nanoparticles are attached to the surface after waiting 24 hours applying the dipping process.

B) Electrical gold nanoparticles trapping

b.1 Trapping set up

The colloids positioning is carried in our trapping station (Fig. 4.16):


Fig 4.16 Trapping station. In this image are shown all the part of the trapping station set up, such as: oscilloscope, function generator, resistance net and connecting box.

As we can observe in the Fig 4.16 the trapping station consists of:

(1) **Function generator Agilent 33250A**: Provides the AC signal necessary for our electrical trapping, in our case will be a square signal.

(2) **Analog Oscilloscope Philips PM 3208 20MHz:** Shows the monitoring signal which is picked up after the sample indicating the trapping case process that we are performing.

(3) **Connecting box:** Allows the connection between the pins of the chip carrier and the trapping devices. Using the different *numbered switches* we select and open the upper pair part of a finger under study making possible the AC signal comes through it passing before through a series resistor (R_s). Two more switches are necessary in our set up: the *shield/down* switch, which opens the down part of the finger and in this way the AC signal flows through the chosen finger towards the oscilloscope and the resistance in parallel (R_p), and the

open switch which connects the *Output* of the function generator with the series resistor and therefore with our electrode.
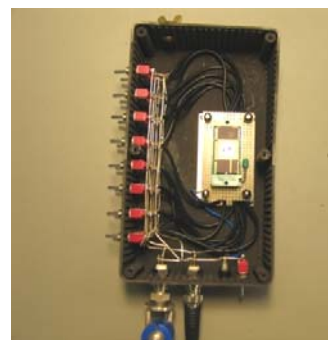
Fig 4.17 Connecting box

(4) **Resistance net:** Rs protects our sample, and modulates the amplitude signal that we are applying. Whereas the parallel resistor (Rp) helps together with the internal oscilloscope resistor, to apply the electrical force to our gold colloids.
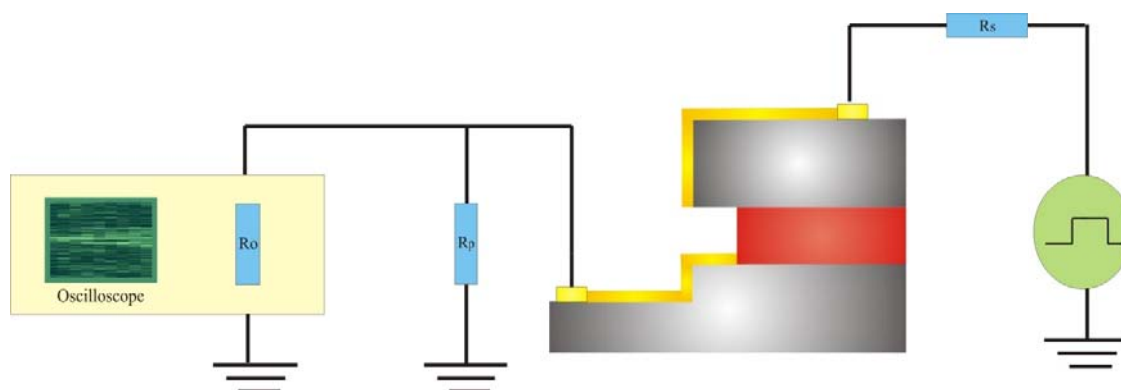
Fig 4.18 Schematic representation of the trapping station. The parts represented are: oscilloscope, function generator, resistance net and the nanogap itself.

An AC signal is required for the process, in our case a square signal is the most suitable one among the signal generator range. The series resistance (R_s) acts a protection of our system and at the same time regulates the induced voltage amplitude in our nanogap.

The resistance in parallel (R_p) with the oscilloscope reduces the value of the internal oscilloscope resistance device resistance ($1M\Omega$), so as the resultant resistance ($R_{eq}=R_o||R_p$), at room

temperature, is pretty lower than the nanogap resistance (R_{gap}) and therefore the dielectrophoresis force is applied in the desirable zone, the electrode region.

- If a *non-trapping case* occurs the signal that currently appears in the oscilloscope (square signal) remains constant. This signal appears on the oscilloscope screen because of the leakage current that flows through our SOI sample and drops in the resistance net.

- If a *hard trapping case* happens, then in the oscilloscope we observe an increment of the initial signal amplitude, since the current flows freely through the gold colloid and now the main voltage drop is at the oscilloscope, which means that an ohmic contact has been created in the system: electrode-Au colloid-electrode, destroying in someway the MCH layer.

- If a soft-*trapping case* takes place no change in amplitude will be monitored, although gold colloidal are trapped in the electrode. The main reason is because at room temperature the leakage current through our system is dominating, so the current through the system Au/MCH/colloid/MCH/Au is negligible.

b.2 Electrical trapping experiments

Next we present the results from the electrical trapping experiments and the followed path in order to achieve the suitable parameters for the soft trapping. As we explained in the last section three types of trapping cases can take place: *non-trapping case*, *hard trapping case* and *soft-trapping*.

The procedure for testing the positioning of gold nanoparticles is based on the following steps:
Firstly and meanwhile the trapping takes place, we make a visual check of the oscilloscope screen, secondly we make an electrical measurement of the sample, testing in this way a possible change in its electrical behaviour regarding the helium reference measurements made in advanced and finally a SEM image is taken from the sample of interest.

If a *non-trapping case* occurs, this implies a non gold nanoparticles assembly in the desirable nanogap region. The signal that appears in the oscilloscope remains constant, and the electrical behaviour regarding to the one taken before starting the electrical trapping does not change. Obviously no gold particles in the nanogap region are expected to appear in the SEM image.
Several *non-trapping case* experiments are presented in the table 4.2. No observable change in the oscilloscope screen is detected in the trapping meantime, and no variation regarding the previous electrical behaviour (helium reference measurements) is noticed.

Non-trapping experiments								
Sample	Voltage (Vpp)	Frequency (Hz)	Time (sec)	Rs (Ω)	Rp(Ω)	SAM	Au (nm)	Result
C76_part1	1	40k	60	1k	4k	None	20	No gold
C76_part1	2	1M	60	1k	4k	None	20	No gold
C79_part1	2.5	250k	60	-	4k	None	20	No gold
C79_part1	2.5	40k	60	1k	1k	None	20	No gold
J8_part1	3.5	85k	180	1k	2k	MCH	60	Gold near the nanogap
J2	3.5	85k	180	1k	2k	OPV$_3$	60	Gold near the nanogap

Table 4.2 Results of non-trapping experiments

The applied voltage range in these experiments is between 1-3.5 Vpp, also several experiments with different frequencies were carried out as well as different resistance nets, SAMs and diameters of gold nanoparticles. The conclusions obtained form this table and after observing the samples in the SEM images are: we need a voltage larger than 3.5 Vpp, so as the threshold voltage for the dielectrophoresis effect to be dominant is reached. The optimum frequency was found to be close to 85 kHz. For the next experiments the time is fixed to 3 minutes and the values for the resistances are fixed to 1kΩ for the serial one and to 2kΩ for the parallel one.
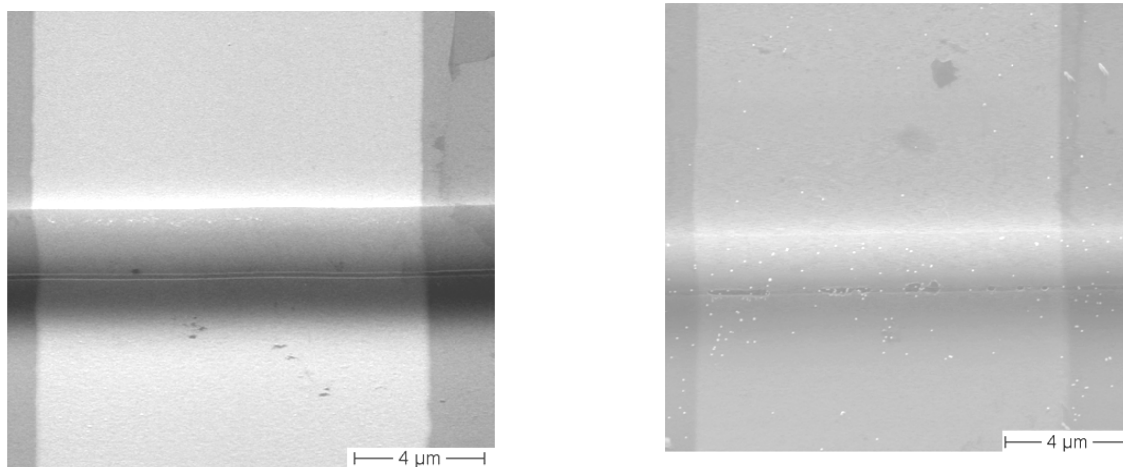
Fig 4.19 Non- trapping case in sample C79_F2 (left) and in sample J2_F23 (right). On the left side, a SEM image taken after the electrical trapping experiments is shown; in this case no gold nanoparticles are situated in the nanogap. On the right, a SEM image after the electrical trapping experiment is shown. In this image we observe how gold nanoparticles appear in the surrounding area of our nanogap, but they are not trapped in the nanogap.
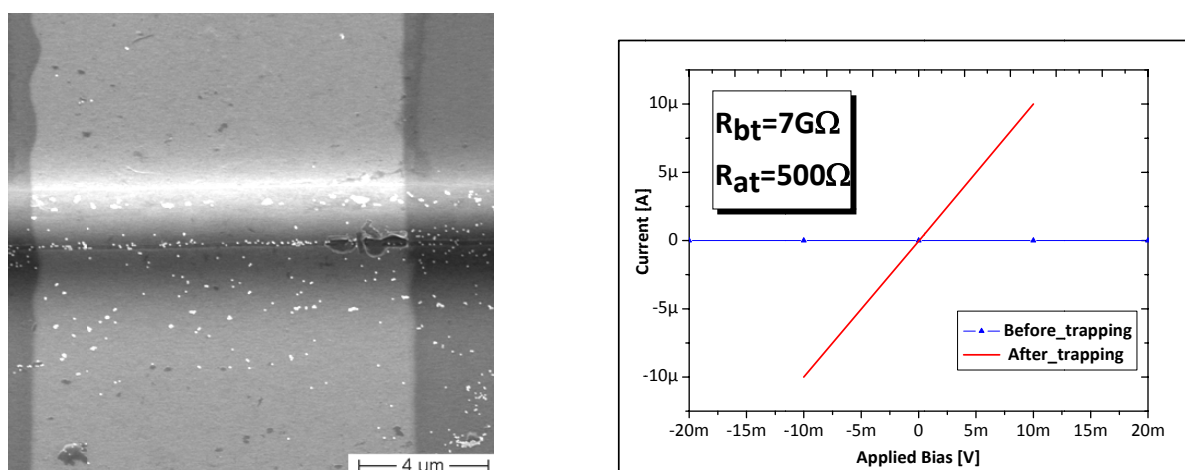
If a *hard-trapping case* happens implies the assembly of gold nanoparticles in the nanogap region, and a *hard* collision between the gold nanoparticles and the electrodes takes place. The signal that appears in the oscilloscope exhibits a clear enlargement in voltage in comparison with its initial amplitude (more than the double amplitude increment with respect the initial amplitude). Also the electrical behaviour regarding to the one measured before starting the electrical trapping (helium reference measurement) changes.

After hard-trapping we obtain an electrical behaviour of the nanogap, corresponding to a lower resistance device. Gold particles are expected to appear in the nanogap region in the SEM image. Several *hard-trapping case* experiments are presented in table 4.3.

Hard trapping experiments								
Sample	Voltage (Vpp)	Frequency (Hz)	Time (sec)	Rs (Ω)	Rp(Ω)	SAM	Au (nm)	Result
C73	7	250k	180	1k	2k	OPV_7	60	Gold in nanogap
J2	8	250K	180	1k	2k	OPV_3	60	Gold in nanogap

**Table 4.3** Results of hard-trapping experiments

In the next figure 4.20 a SEM image and the electrical behaviour of our nanogap in which a hard trapping has been performed, are presented.

Fig 4.20 Hard trapping case in sample C73_F24. On the left side, a SEM image taken after the electrical trapping experiments is shown. Gold nanoparticles in the nanogap region and also in the surrounding area are visible. On the right side, the electrical behaviour before and after the electrical trapping experiment is shown, in this graphic we see a change in the resistance of our device from 7 GΩ to 500Ω.

If a *soft-trapping case* occurs it means that assembly of the gold nanoparticles has been achieved, without a hard collision between the gold nanoparticles and the electrodes. There is no change in the signal that appears in the oscilloscope and after a soft-trapping we obtain a behaviour corresponding to either Coulomb blockade or Coulomb blockade staircase. Gold particles are expected to appear in the nanogap region, in the SEM image.

Next we present in figure 4.21 two SEM images where a successful gold nanoparticles assembly was achieved.
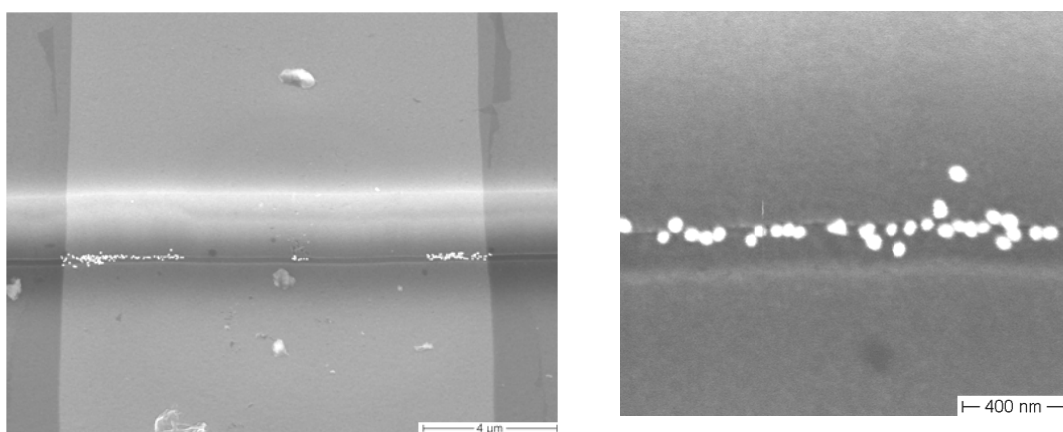
Fig 4.21 Soft trapping case in sample C7_F23. On the left image it is shown a SEM image taken after the trapping experiments where gold nanoparticles are placed in the nanogap region. On the right SEM image we see a detail of the left image, where 60 nm gold particles are visibly trapped in the nanogap.

The trapping parameters which were used for the successful soft trapping are the following:

- **Voltage:** 4V
- **Frequency:** 85 KHz
- **Time of trapping:** 180sec
- **Rs:** 1 kΩ
- **Rp:** 2 kΩ
- **SAM**: OPV_7
- **Gold nanoparticle**: 60nm (diameter)

Chapter 5

Transport measurements in a two-junction system

In the first part of this chapter theoretical concepts such as Coulomb blockade and Coulomb blockade staircase are explained.

In the second part of the chapter the results of the transport measurement carried out in our two-junction system are presented and analyzed.

5.1 Coulomb blockade

5.1.1 Fundamental theoretical concepts

"How small and how cold should a conductor be so that adding or subtracting a single electron has a measurable effect?" This is the starting point for the theoretical explanation about Coulomb blockade effect

On the one hand and due to our system size we find the concept of *energy quantization*:

If the *deBroglie wavelength* of the electrons is comparable to the size of the quantum dot, the electrons occupy discrete quantum levels (splitting) similarly to the atomic orbitals in atoms and therefore they have a discrete energy excitation spectrum.

The deBroglie hypothesis is the statement which claims:"All matter has a wave-like nature (wave-particle duality)". The deBroglie relationships show that the wavelength is inversely proportional to the momentum of a particle.

$$\lambda = \frac{h}{p} = \frac{h}{\gamma m v} = \frac{h}{m v} \sqrt{1 - \frac{v^2}{c^2}}$$

[5.1]

In the case of an electron, the deBroglie wavelength is: 1.226 nm, so as our metallic quantum dot is in the range of 30 nm we can assert we have hardly energy level quantization in the dot, so the level splitting is not relevant in our case.

On the other hand and due to our system temperature we find the concept of *temperature regime:*

The Coulomb interaction, depicted as **e^2/C**, is a fundamental concept which makes comprehensible the explanation of our system behaviour.

The capacitance factor (**C**) parameterizes the Coulomb interactions between the electrons in the dot and between electrons in the dot and those in our gold electrodes. These energy interactions are modelled by the basic capacitance concept (measurement of the electric charge amount, stored, for a given electric potential):

$$C = \frac{Q}{V} [F]$$

[5.2]

So the change in the potential is:

$$V = \frac{Q}{C} \, [V]$$

[5.3]

Since the charge is quantized is in units of e:

$$V = \frac{e}{C} \, [V]$$

[5.4]

And if we transfer it to energy units:

$$eV = \frac{e^2}{C} \, [J]$$

[5.5]

Then **e²/C** is the Coulomb energy, also known as charging energy is changed, and shows if an additional charge *e* is introduced in our system, and therefore the electrostatic potential is also modified by this amount of energy. This charging energy should be higher than the thermal energy, otherwise the electron transitions could be also originated by thermal fluctuations and the Coulomb effect would be hidden.

$$\frac{e^2}{C} \gg k_B T$$

[5.6]

So this condition is able to be fulfilled when we have got small capacitances and also when we are at a very low temperature.
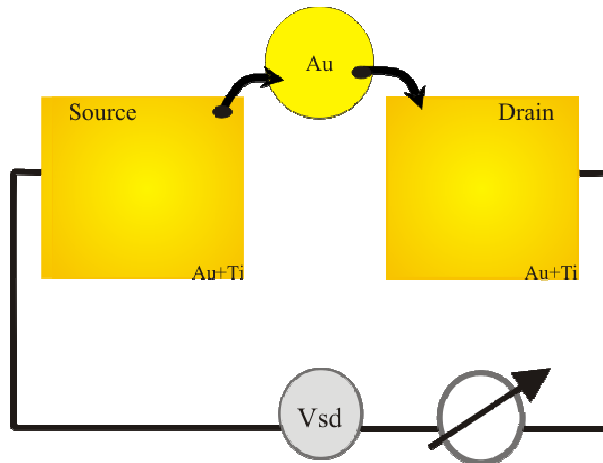
In our system we are in the classical Coulomb blockade regime .This regime is determined by the temperature range:

$$\Delta E' \ll k_B T \ll \frac{e^2}{C}$$

[5.7]

Where $\Delta E'$ is defined as quantum mechanical level splitting.

5.1.2 The Coulomb blockade system

The following picture shows a sketch of our system:

Fig 5.1 System under study. Schematic representation of our system, where we distinguish the two leads of gold titanium, the trapped nanoparticle and the voltage source.

Electrons can tunnel between the terminals, as indicated by the arrows. These source and drain terminals connect the small isolated particle in our case the gold colloidal to macroscopic current and voltage meters [1, 2].

Our small particle acts as an island for electrons and the number of electrons on this island is an integer number *N,* so we assume the charge on the island is quantized and equal to *Ne*. If we allow tunnelling to the source and drain electrodes, the number of electrons *N* adjusts itself until the energy of the whole circuit is minimized. When tunnelling occurs, the charge on the island suddenly changes by the quantized amount *e*.

The states in the leads are filled up to the electrochemical potentials μ_{left} and μ_{right} which are connected via the externally applied source-drain voltage. (V_{sd} = (μ_{left} - μ_{right})/e) .The number of available states in the dot follows from calculating the electrochemical potential μ_{dot} (N). This is, by definition, the minimum energy for adding the N_{th} electron to the dot:
μ_{dot} (N) =U (N)-U (N-1), where *U (N)* is the total ground state energy for *N* electrons on the dot at zero temperature.
We are in the most simplify model, in which we have assumed the Coulomb interactions among the electrons in the dot and between electrons in the dot and those somewhere else in the environment are represented by a capacitance *C*. And in which this C is independent of the number of electrons on the dot. All these assumptions lead to the following description for µ*dot (N):*

$$\mu_{dot}(N) = E_N + \frac{(N - N_0 - \frac{1}{2})e^2}{C}$$

[5.8]

Where E_N=*chemical* potential (μch $(N) = E_N$)

> N=Number of electrons that enters the system
> N_0=Number of electrons that were in the system
> e^2/C = charging energy due to an electron

When the number of electrons is changed by one, the resulting change in electrochemical potential in our system is:

$$\mu_{dot}(N+1) - \mu_{dot}(N) = \Delta E' + \frac{e^2}{C}$$

[5.9]

In our system quantum mechanical level splitting is no relevant: $\Delta E' = E_{N+1} - E_N \sim 0$

Once the components of our system are defined, we should focus on the tunnelling aspects.
At zero temperature transport occurs according to the following rule: *current is (non) zero when the number of available states on the dot in the energy window between* μ_{left} *and* μ_{right} *is (non) zero*. So non-zero addition energy can lead to a blockade for tunnelling of electrons on and off the dot, as depicted in the following sketch where *N* electrons are localized on the dot.
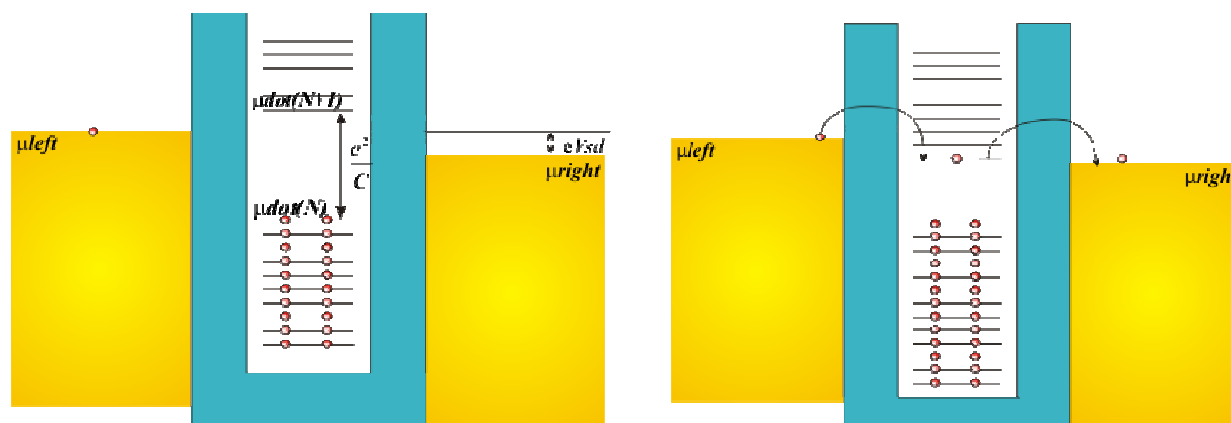
Fig 5.2 Coloumb blockade scenario. On the left image the electron cannot tunnel on the island, because there are no available levels between the two leads. On the right image on increasing Vsd, current starts flowing when levels appear between the two leads.

In the left image the *(N+1)* th electron cannot tunnel on the dot, because the resulting electrochemical potential μ_{dot} *(N+1)* is higher than the potentials of the reservoirs.

So, for μ_{dot} *(N)* < μ_{left}, μ_{right} < μ_{dot} *(N+1)* the electron transport is blocked, which is known as the **Coulomb blockade**. In this condition the tunnelling current is zero as long as the interval between μ_{left} and μ_{right} does not contain a charge state.

On increasing V_{sd}, current starts flowing when either μ_{left} > μ_{dot} *(N+1)* or μ_{dot} *(N)* > μ_{right}, *depending* on how the voltage drops across the two barriers. One can think of this as opening a charge channel, corresponding to either the N $\rightarrow$ *(N+1)* or *(N-1)* $\rightarrow$ *N* transition [6, 7].

5.1.3 Coulomb blockade staircase

When two tunnel barriers appear in a system, two different cases can be observed depending on the ratio of the resistances and capacitances of the two junctions. This parameter ratio defines our junction widths and therefore gives us information about each tunneling junction, which can have different or identical values for resistances and/or capacitances.

1st) Case: **Coulomb blockade** behavior, which has been previously explained and implies a reduced current around zero bias. This effect is dominant and appears when the two tunnel barriers have identical parameter ratio ($R_1C_1=R_2C_2$).

2nd) Case: **Coulomb staircase**: If a strong asymmetry exists in the parameter ratio that is, the product for the parameter junctions is very different ($R_2C_2 \gg R_1C_1$) a Coulomb staircase with sharp steps is expected. This staircase is translated into a non-linear transport *I-V$_{sd}$* behavior and arises from the incremental increase in the current at voltages where it is energetically favorable for an additional electron to sit on the middle electrode [3].

This is in agreement with the orthodox single-electron tunneling theory [4], which assumes a continuous density of states for the cluster. The following circuit *Fig 5.3* shows a schematic of our experiment, in which each of the tunnel barriers are modelled as a parallel capacitor and a resistor:
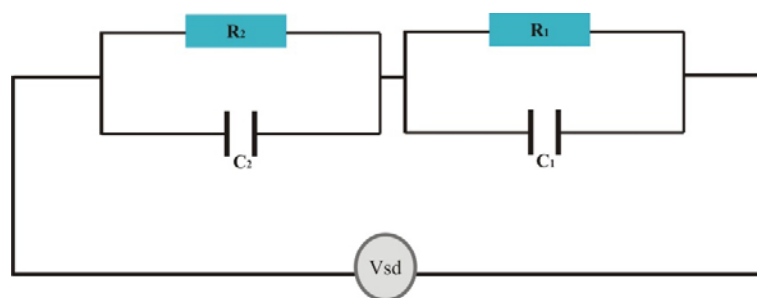

Fig 5.3 Schematic of our experiment. Each tunnel barrier is depicted as a resitance and capacitance in parallel.

The values of these electrical components which parameterize our system will be discussed in the next section.

In the so-called *Coulomb staircase*, the electrochemical potential of one of the reservoirs is essentially fixed relative to the charge states in the dot, while the electrochemical potential of the other reservoir moves in accordance with V_{sd}. In this asymmetric case, the current changes are expected to appear in the characteristics as pronounced steps.

In the following energy diagram, figure 5.4, we can observe a case with asymmetrical tunnel barriers. It is clear that for larger source-drain voltages V_{sd} *the* empty states above the Coulomb gap can be occupied. This can result in a Coulomb staircase in current voltage characteristic.
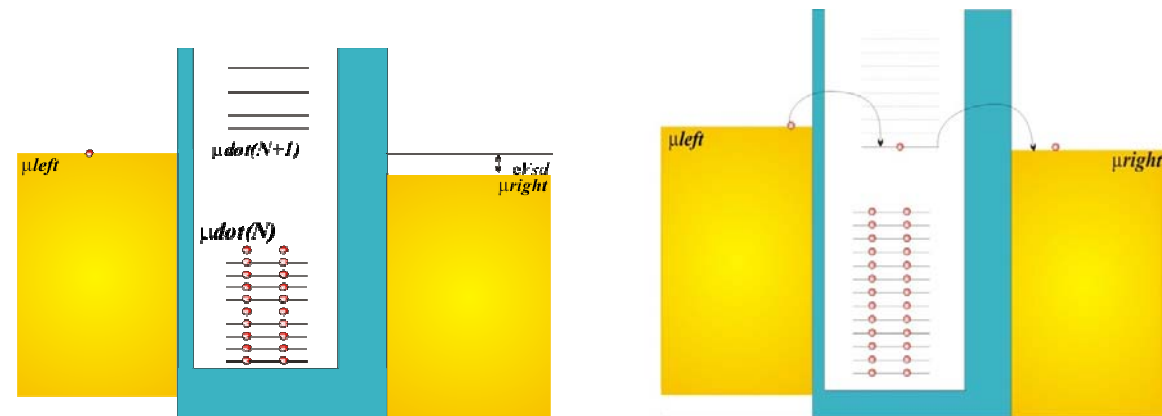
*Fig 5.4 Coloumb blockade staircase scenario.*On the left image the electron cannot tunnel on the island, because there are no available levels between the two leads. On the right image on increasing Vsd, current starts flowing when levels appear between the two leads. In this case we observe how the tunnel barriers are asymmetrical. If an asymmetry exists between the tunnel barriers a Coulomb staircase with sharp steps is expected.

5.1.4 Variation of the Coulomb blockade staircase

As in the theoretical studies presented in the work of *A.Hanna & M.Tinkham and M. Amman and R. Wilkins* [5,6] a qualitative estimation can be carried out for our Coulomb staircase data, being able in this way to determine the individual parameters of the two-junction system[7,8,9]. Next the mathematical derivations presented in the referenced [5, 6] will be reviewed.

The key parameters for a good characterization of our system, such us capacitances (C_1, C_2), resistances (R_1, R_2) and the fractional residual charge (Q_0), from the tunnel barriers, can be obtained from the I-V curve of our system. As we have already mentioned the capacitances and resistances which belong to the tunnels junctions are known as parameter ratio and model the tunnel junction, whereas Q_0 represents the fractional electron charge present in our particle (in our case the conductive nanocolloid) when the electrodes are floating (before applying voltage). This fractional charge is the residual one on the cluster and it is thought to be originated by the

difference in the work functions of the metals used in our junctions, in our case gold (nanocolloid) and titanium-gold (electrodes).

The starting point for a thorough study about features and variation of the Coulomb blockade staircase is the tunnelling resistance ratio r $=R_2/R_1$. The assumption for this relation is $R_2/R_1 >>1$, owing to the asymmetry in the tunnel junctions.

It is possible to obtain a simple analytical expression for the current flowing in our system: I (V), considering $r >>1$, this assumption involves a relation between the tunnelling rate of: $\Gamma_1 >> \Gamma_2$

The particle tunnel rate for the junction j[th] is represented by [5]:

$$\Gamma_j(n) = \frac{1}{R_j e^2}\left(\frac{-\Delta E_j^{\pm}}{1-\exp(\Delta E_J^{\pm}/k_B T)}\right)$$

[5.10]

Where $\Delta E_j^{\pm}$ is the energy change of the system when the electron tunnels across the barrier and R_j is the tunnel resistance of the jth junction.

The current in the system is given by:

$$I(V) = e\sum_{n=-\infty}^{\infty}\sigma(n)\left[\Gamma_2^+(n)-\Gamma_2^-(n)\right] = e\sum_{n=-\infty}^{\infty}\sigma(n)\left[\Gamma_1^+(n)-\Gamma_1^-(n)\right]$$

[5.11]

Where $\sigma(n)$ is the ensemble distribution of the number of electrons on the center electrode. The most probable number of electrons on the centre electrode, $n=n_0$, is primary determined by junction one because: $\Gamma_1 >> \Gamma_2$, this also means: $\sigma(n_0) \geq \sigma(n_0 \pm 1)$. In this way the ensemble distribution for the number of electrons in the middle electrode has a higher or equal value than for the number of electrons that are outside the electrode.

So taking this condition in the distribution we obtain two sub-conditions for obtaining the limits for n_0 within the concept of maximum probability.

$$\boxed{\sigma(n_0) \geq \sigma(n_0 \pm 1)} \qquad \begin{cases} \sigma(n_0) \geq \sigma(n_0+1) & \textbf{(a)} \\ \sigma(n_0) \geq \sigma(n_0-1) & \textbf{(b)} \end{cases}$$

The ensemble distribution $\sigma(n)$ is obtained by noting that the net probability for making a transition between any two adjacent states *in steady state* is zero:

$$\sigma(n)\left[\Gamma_1^+(n) + \Gamma_2^+(n)\right] = \sigma(n+1)\left[\Gamma_1^-(n+1) + \Gamma_2^-(n+1)\right]$$

[5.12]

So from $\Gamma_1 \gg \Gamma_2$ we obtain that:

$$\sigma(n)\left[\Gamma_1^+(n)\right] = \sigma(n+1)\left[\Gamma_1^-(n+1))\right]$$

[5.13]

Now we apply the sub-conditions (a) and (b):

(a) If $\sigma(n_0) \geq \sigma(n_0 + 1) \longrightarrow \quad \Gamma_1^-(n_0 + 1) \geq \Gamma_1^+(n_0)$

From the equation which describes the particle tunnel rate:

$$\frac{1}{R_1 e^2}\left(\frac{-\Delta E_1^-(n_0 + 1)}{1 - \exp(\Delta E_1^-(n_0 + 1)/k_B T)}\right) > \frac{1}{R_1 e^2}\left(\frac{-\Delta E_1^+(n_0)}{1 - \exp(\Delta E_1^+(n_0)/k_B T)}\right) \quad [5.14]$$

In where:

ΔE_1^- <0, because we remove charge, so the energy decreases.
ΔE_1^+ >0, because we add charge, so the energy increases.

Also we consider the hypothesis $|\Delta E_1| \gg k_B T$, where the energy change of the system is higher than the thermal energy **($k_B T$)**.
So analyzing the factors from both sides of the equation 4.23:

$$\alpha = \left(\frac{-\Delta E_1^-(n_0 + 1)}{1 - \exp(\Delta E_1^-(n_0 + 1)/k_B T)}\right) \Rightarrow \text{if we take the exponential part from the denominator}$$

and we apply the conditions: ΔE_1^- <0 and $|\Delta E_1| \gg k_B T$ then $\exp(\Delta E_1^-(n_0 + 1)/k_B T) \cong 0$

$$\boxed{\alpha = -\Delta E_1^-(n_0 + 1)}$$

In the same way:

$$\beta = \left(\frac{-\Delta E_1^+(n_0)}{1 - \exp(\Delta E_1^-(n_0)/k_B T)} \right) \Rightarrow \text{ if we take the exponential part from the denominator}$$

and we apply the conditions: $\Delta E_1^+ > 0$ and $\left| \Delta E_1 \right| \gg k_B T$ then ($\exp(\Delta E_1^-(n_0 + 1)/k_B T) \cong \infty$

$\boxed{\beta = 0}$

So $0 < -\Delta E_1^-(n_0 + 1)$, and now we apply the equation obtained from electrostatic energy consideration, which describes the energy change of the system:

$$\Delta E_1^{\pm} = \frac{e^2}{C_\Sigma} \left(\frac{e}{2} \pm (ne - Q_0) \pm C_2 V \right)$$

[5.15]

In this case:

$$0 < -\left(\frac{e^2}{C_\Sigma} \left(\frac{e}{2} - (ne - Q_0) - C_2 V \right) \right) \text{ with } n = (n_0+1); \text{ so we obtain the lower limit for } n_0 \text{ (most}$$

probable number of electrons on the center electrode):

$$n_0 > \left(-\frac{e}{2} + Q_0 - C_2 V \right) \frac{1}{e}$$

[5.16]

(b) If $\sigma(n_0) \geq \sigma(n_0 - 1) \longrightarrow \Gamma_1^+(n_0 - 1) \geq \Gamma_1^-(n_0)$

From the equation which describes the particle tunnel rate:

$$\frac{1}{R_1 e^2} \left(\frac{-\Delta E_1^+(n_0 - 1)}{1 - \exp(\Delta E_1^+(n_0 - 1)/k_B T)} \right) > \frac{1}{R_1 e^2} \left(\frac{-\Delta E_1^-(n_0)}{1 - \exp(\Delta E_1^-(n_0)/k_B T)} \right)$$

[5.17]

Following the same mathematical procedure as with condition (a) we obtain in this case:

$$0 > -\left(\frac{e^2}{C_\Sigma}\left(\frac{e}{2} - (ne - Q_0) - C_2 V\right)\right)$$ with *n= (n₀+1)*; so we obtain the upper limit for *n₀* (most probable number of electrons on the center electrode):

$$n_0 < \left(\frac{e}{2} + Q_0 - C_2 V\right)\frac{1}{e}$$

[5.18]

If we put together lower and upper limits for *n₀*:

$$e^{-1}\left(-C_2 V + Q_0 - \frac{e}{2}\right) \leq n_0 \leq e^{-1}\left(-C_2 V + Q_0 + \frac{e}{2}\right)$$

[5.19]

Subtracting both limits we find that the difference is "1" (an integer) so this result implies that *n₀* is also an integer and jumps each time by one. This result leads us to the following conclusion for the ensemble distribution of the number of electrons on the center electrode: $\sigma(n) \approx \delta_{n,\,n0}$,

since the normalization condition $\sum_{n=-\infty}^{\infty} \sigma(n) = 1$ is satisfied by the Dirac delta function.

The current is given then by:

$$I(V) = e\left[\Gamma_2^+(n_0) - \Gamma_2^-(n_0)\right]$$

[5.20]

Another conclusion from the limits of *n₀* is extracted ; this is that the charge in the system (*Q=ne-Q₀*) jumps from:

$$\left(-C_2 V - \frac{e}{2}\right) \leq en_0 - Q_0 \leq \left(-C_2 V + \frac{e}{2}\right)$$ [5.21]

$$\left(-C_2 V - \frac{e}{2}\right) \leq Q \leq \left(-C_2 V + \frac{e}{2}\right)$$ [5.22]

Considering the next hypothesis $\left|\Delta E_2^\pm(n_0)\right| \gg k_B T$, and if the temperature is low enough, the inferred expression for Γ₂*(n₀)* is :

$$\Gamma_2^{\pm}(n_0) = \left\{ \frac{1}{R_2 C_{\Sigma}} \left[-\frac{1}{2} \mp (n_0 - Q_0/e) \pm C_1 V/e \right], \text{for } \Delta E_2^{\pm} < 0 \right.$$

$$\text{and } \Gamma_2^{\pm}(n_0) = 0 \text{ for } \Delta E_2^{\pm} > 0$$

This means that *I(V)=0*, and therefore we observe the *Coulomb blockade* in the region where the voltage is within the next range:

$$\boxed{(-e/2 + n_0 e - Q_0)/C_1 \leq V \leq (e/2 + n_0 e - Q_0)/C_1} \qquad [5.23]$$

Valuable features of our data are identified by means of the achieved conditions (Eq. 5.20 and Eq. 5.23) for the most probable number of electrons on the center electrode and the for *I (V)=0* respectively.

So depending if the voltage reaches the limits in (Eq. 5.19) or in (Eq. 5.23) two behaviors are showed:

- If there is a change in n_0 implies the voltage attains the limit in (Eq. 5.19) and we will observe a discrete jump in the current. So the most probable number of electrons in the middle of the electrode is determined by junction 1, which has a much higher tunneling rate (Γ_1).

- Nevertheless if the voltage goes beyond the Coulomb blockade limits (Eq. 5.23) then we observe a linear enlarge in current. So the smaller tunneling rate (Γ_2) responds to this constant n_0 by adjusting the current.

We can identify also for which values in voltage occur the first changes in our staircase, either a step or a linear increase in the current:

In order to get the thresholds voltages we should estimate the value of n_0 in the very beginning, when the applied voltage is "0":

So taking into account equation 5.20:

$$\boxed{e^{-1}\left(-C_2 V + Q_0 - \frac{e}{2}\right) \leq n_0 \leq e^{-1}\left(-C_2 V + Q_0 + \frac{e}{2}\right)}$$

And if *V=0*, then:

$$\left(+Q_0 - \frac{e}{2}\right) \le n_0 \le \left(+Q_0 + \frac{e}{2}\right)$$ and dividing by e the limits:

We obtain that: n_0 is equal to "0" for a voltage equal to "0".

Explanation

The number n_0 is the integer nearest $\dfrac{Q}{e}$ and $\left|\dfrac{Q_0}{e}\right| \le \dfrac{1}{2}$ since:

$Q = ne - Q_0$ and if we make: $\dfrac{Q}{e} = n - \dfrac{Q_0}{e}$. Let us suppose that $\dfrac{Q}{e} = 7.3$, then n=7(the integer

nearest) and $\dfrac{Q_0}{e}$ =-0.3, so $\left|\dfrac{Q_0}{e}\right| \le \dfrac{1}{2}$.

In this case $-0.8 \le n_0 \le 0.2$ so $n_0=0$.

THRESHOLD VOLTAGES:

A) $e^{-1}\left(-C_2V + Q_0 - \dfrac{e}{2}\right) \le n_0 \le e^{-1}\left(-C_2V + Q_0 + \dfrac{e}{2}\right)$

From this equation we obtain the first thresholds in voltage where we can observe a discrete jump in the current:

$$-C_2V - \frac{e}{2} \le en_0 - Q_0 \le -C_2V + \frac{e}{2}$$ with $n_0=0$

$$-C_2V - \frac{e}{2} \le -Q_0 \le -C_2V + \frac{e}{2}$$

So the down voltage threshold (V_{thdJ}) and the up voltage threshold (V_{thuJ}) are:

$$V_{thdJ} \le \frac{+Q_0 - \dfrac{e}{2}}{C_2} \quad \text{and} \quad V_{thuJ} \ge \frac{+Q_0 + \dfrac{e}{2}}{C_2}$$

B) $\left(-e/2 + n_0 e - Q_0\right)/C_1 \leq V \leq \left(e/2 + n_0 e - Q_0\right)/C_1$ with $n_0 = 0$

From this equation we obtain the first thresholds in voltage where we can observe a linear enlarge in current.

$$V_{thdL} \leq \frac{-\dfrac{e}{2} - Q_0}{C_1} \quad \text{and} \quad V_{thuL} \geq \frac{+\dfrac{e}{2} - Q_0}{C_1}$$

- The difference between both thresholds is: $\dfrac{e}{C_2}$

- The sum between both thresholds is: $\dfrac{2Q_0}{C_2}$

The current outside the Coulomb-blockade region is given by the next equation:

$$I(V) = \frac{1}{R_2 C_\Sigma}\left(-(n_0 - Q_0) + C_1 V - \frac{e}{2}\operatorname{sgn}(V)\right) \quad [5.24]$$

This equation shows us that the plateau slope on a step with n_0 constant and it is equal to $\dfrac{C_1}{R_2 C_\Sigma}$, since in a line expressed in the Cartesian plane, in two dimensions, the characteristic equation is often given by the *slope-intercept form*:

$$y = mx + b$$

And in this equation we can identify m as the slope of the line.

Taking into account the positive and negative voltages separately, four cases are distinguished in the next phase diagram. In this diagram we can make a qualitative analysis by noting the sequence of conduction starts.
So once we have placed our I-V data in one of the cases region, we can proceed to determine the model parameters of our two-tunnel barrier system.
In the next phase diagram four different cases are distinguished, each of them with different onset in conduction.
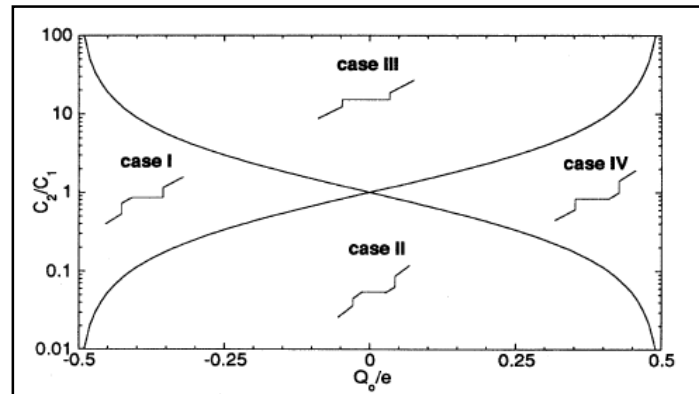
Fig 5.5 Phase diagram of the four qualitatively different cases of I-V curves [5]. Within each case is shown a small trace which is representative of data in that region, although the shape of the trace can be varied greatly within each case by changing Q_0 or C_2/C_1.

We have chosen the **Case II** for illustration by means of a simulation the different onsets of conduction and the different threshold voltages.

- $V_{thdJ} \leq \dfrac{+Q_0 - \dfrac{e}{2}}{C_2}$ and $VthuJ \geq \dfrac{+Q_0 + \dfrac{e}{2}}{C_2}$ discrete jump in the current.

- $V_{thdL} \leq \dfrac{-\dfrac{e}{2} - Q_0}{C_1}$ and $VthuL \geq \dfrac{+\dfrac{e}{2} - Q_0}{C_1}$ linear increase in current.
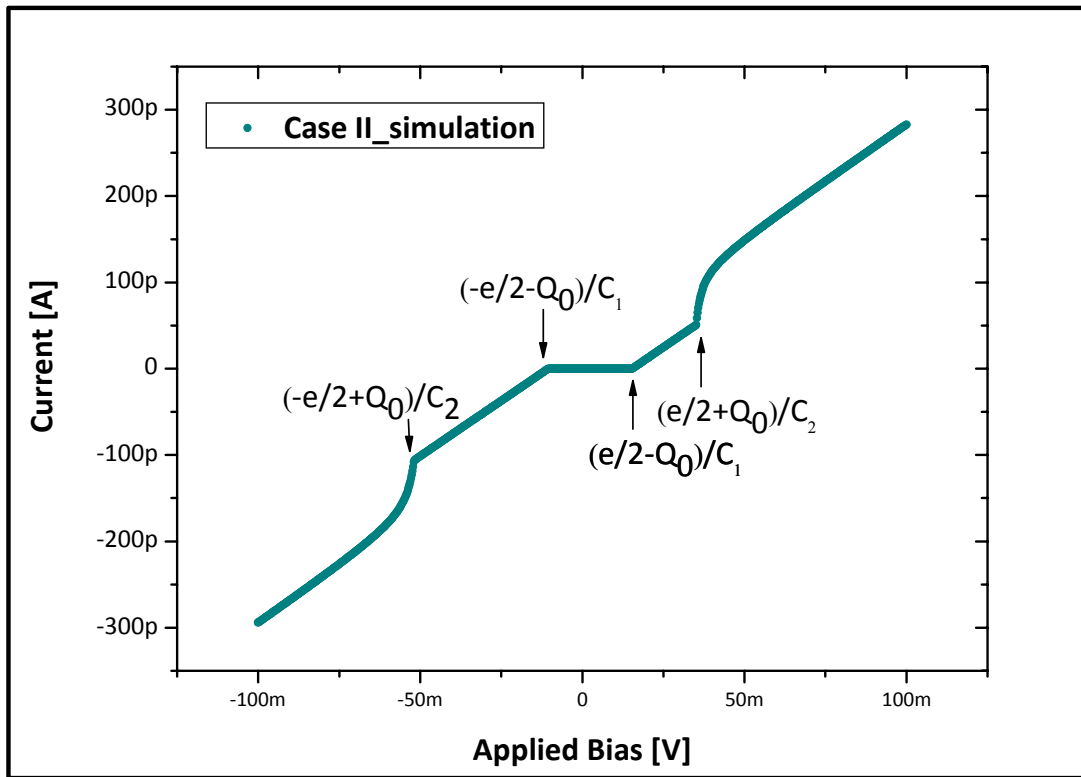
Fig 5.6   I-V curve simulation of Case II The parameters used for the simulation are: C_1=13.6 aF, C_2= 4.05aF, R_1=0.3 MΩ, R_2=29.3 MΩ and Q_0=-0.096e [10].

5.2 Transport measurements

5.2.1 Coulomb blockade

In this section we present a soft-trapping experiment where exists a Coulomb blockade situation. Firstly in figure 5.7 we present three SEM images where gold nanoparticles can be observed in the nanogap region.
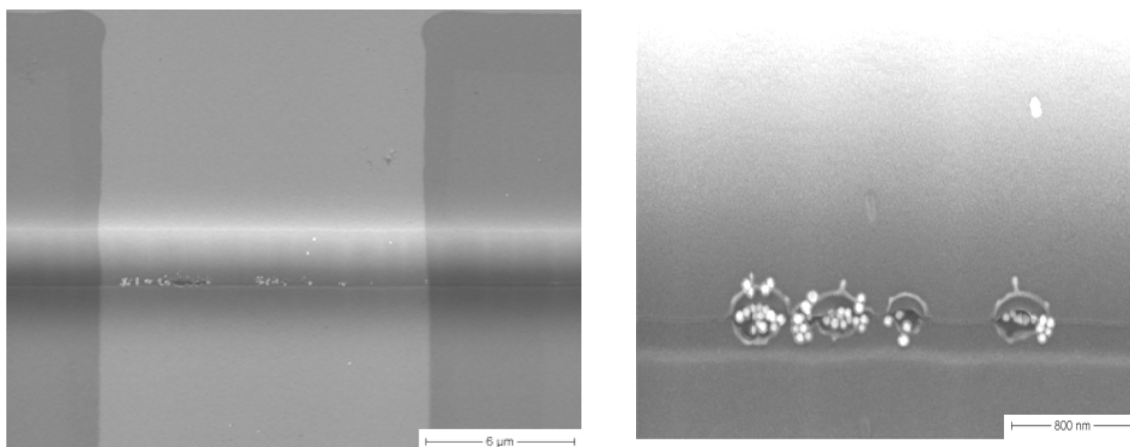
Fig 5.7 SEM images of a soft trapping case of sample J8_part1_f22.The parameters for the electrical trapping are the following: voltage: 4V, the frequency: 85 KHz, the time of trapping: 180sec, Rs: 1 kΩ, Rp: 2 kΩ, SAM: MCH and Gold nanoparticle: 60nm (diameter).The circular features observed in the nanogaps region are caused once we applied, after the gold nanoparticle trapping, a certain amount of voltage and therefore due to the conduction effect some part of the gold which covered the electrodes is melted and forms circular shapes.

In the next figure we present the electrical behaviour of our nanogap, before and after the electrical trapping experiment, it is visible the electrical change in the resistance of our device. The initial resistance measured in our nanogap was of 52.5 GΩ.
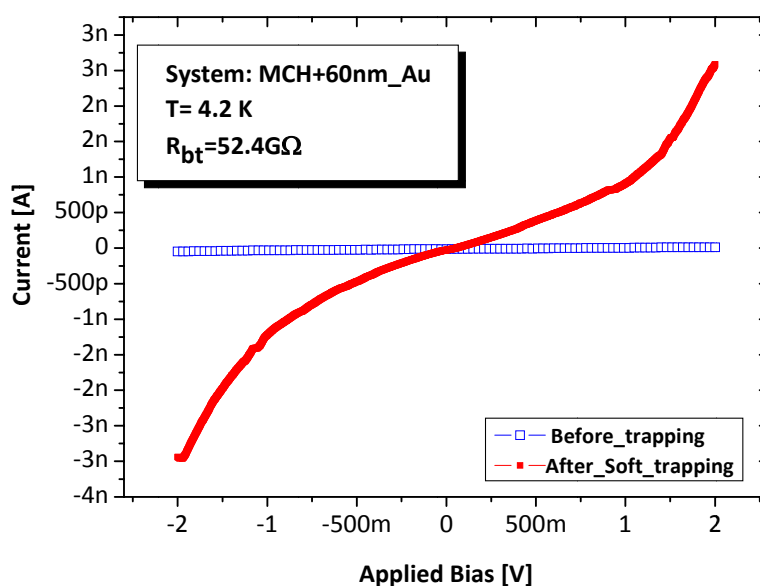
Fig 5.8 I-V characteristic of Coulomb blockade effect. We observe a reduced current around zero applied bias with respect of the rest of the graphic. This effect is dominant when the parameters of our two-junction system are $R_1C_1=R_2C_2$.
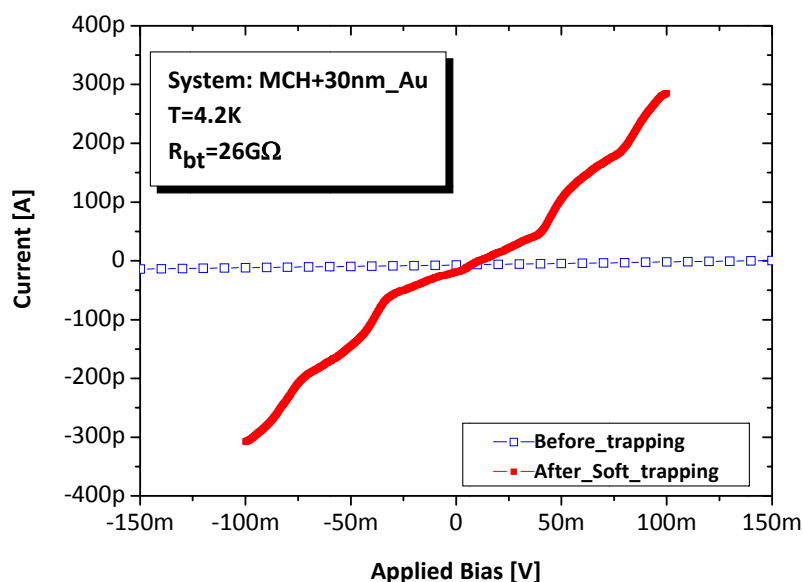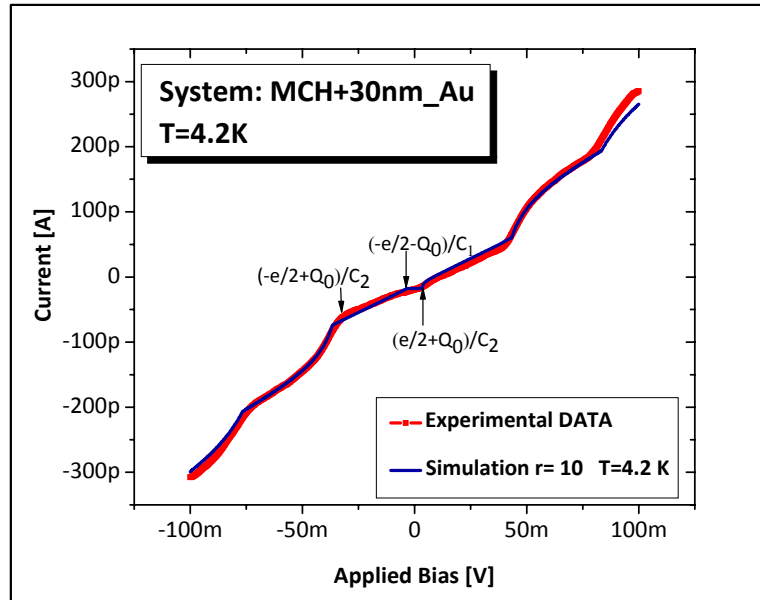
5.2.2 Coulomb blockade staircase

In this section we present a soft-trapping experiment where exists a Coulomb blockade staircase situation. Firstly in the figure 5.9, we present two SEM images where gold nanoparticles can be observed in the nanogap region
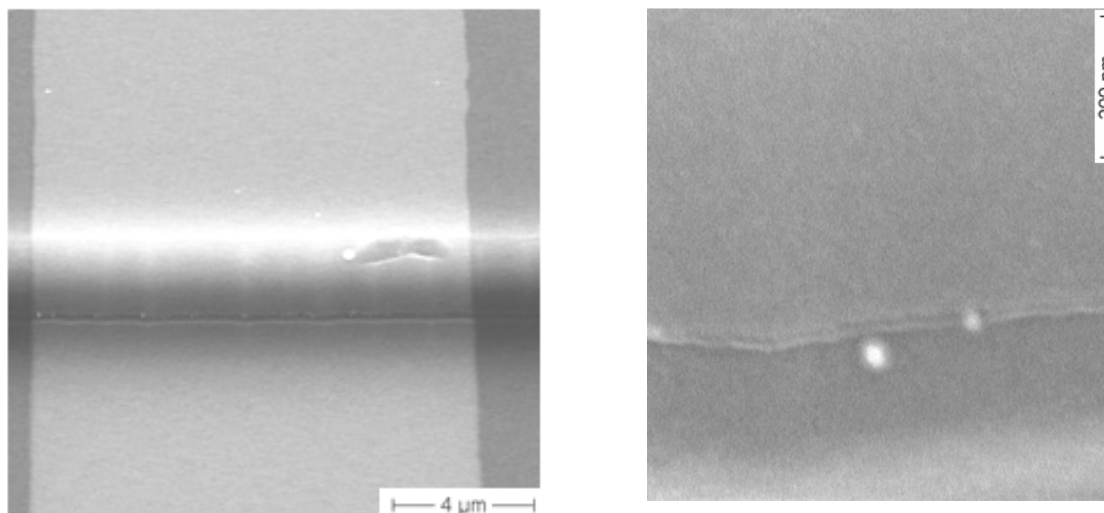
Fig 5.9 SEM images of a soft trapping case of sample J6_part1_f16.The parameters for the electrical trapping are the following: voltage: 4V, the frequency: 85 KHz, the time of trapping: 180sec, Rs: 1 kΩ, Rp: 2 kΩ, SAM: MCH and Gold nanoparticle: 30nm (diameter) .On the right image we observe a detail of the left SEM image region where we distinguish a nanoparticle inside and outside the nanogap region.

In the next figure we present the electrical behaviour of our nanogap, before and after the electrical trapping experiment, it is visible the electrical change in the resistance of our device. The initial resistance measured in our nanogap was of 26 GΩ.

Fig 5.10 I-V characteristic of Coulomb blockade staircase effect. We observe a non-linear I-V behavior, this effect is dominant when the parameters of our two-junction system are $R_1C_1<<R_2C_2$.

Accordingly the phase diagram in Fig. 5.5 and observing the conducting onsets we are in the Case I. Once we have calculated the parameter s of our two junction system we proceed to make the corresponding simulation with the software developed by Korotkov *and Likarev* [7]:

Fig 5.11 I-V characteristic of Coulomb blockade staircase effect. We compared the non-linear I-V behavior of the experimental data with the software simulation. The kinks of our staircase, which tell us about the parameters of our two-junction system are also depicted in the image [10]

The corresponding derivative from the measured Coulomb blockade staircase is depicted in the Figure 5.12:
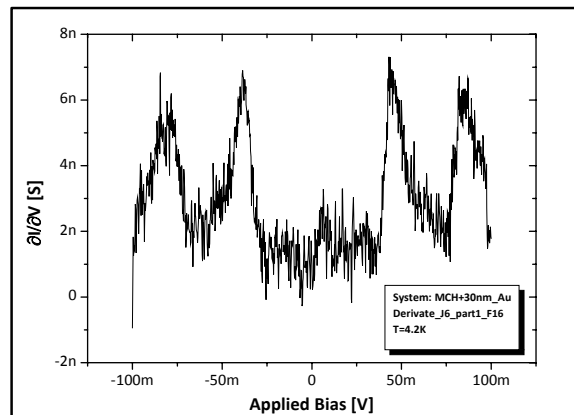
Fig 5.12 Derivative behavior of the Coulomb blockade staircase data. We observe in this derivative graphic the position of the different kinks of the Coulomb blockade staircase.

The thresholds voltage where we can observe a discrete jump in the current are given by

$$V_{thdJ} \leq \frac{+Q_0 - \frac{e}{2}}{C_2} \quad \text{and} \quad V_{thuJ} \geq \frac{+Q_0 + \frac{e}{2}}{C_2}$$

So extracting this voltage values from our data (Fig 5.11) we obtain:

$$\frac{+Q_0 + \frac{e}{2}}{C_2} = 3mV \quad \text{and} \quad \frac{+Q_0 - \frac{e}{2}}{C_2} = -33mV \text{ so if we subtract the upper threshold voltage}$$

from the lower threshold voltage we obtain:

- $\dfrac{e}{C_2} = 36mV$

- $\dfrac{2Q_0}{C_2} = -30mV$

C_2=4.45 aF and for Q_0= -0.4166e

And the value of the capacitor C_1 is given by the equation 5.23 concretely by expression:

$$V_{thdL=} \frac{-\frac{e}{2} - Q_0}{C_1} = -3mV \text{ and therefore } C_1 \text{ it is equal to: } C_1 = 4.45 \text{ aF.}$$

The values for the resistance R_2 are obtained from the plateau slope on a step when n_0 constant and it is equal to $\dfrac{C_1}{R_2 C_\Sigma}$.

So in our case as $C_1 = C_2$ then the slope is equal to $\dfrac{1}{2R_2}$ and extracting the plateau slope on a step from the measured data we have the next values for the resistances in our two- junction system:

R_2= 300 MΩ and assuming R2>>R1 and r= 10, then R_1=30MΩ.

To see the effect of the ratio r =R_2/R_1 in the discrete jumps of current we made a simulation with r=∞ , and with a temperature of T=0, in comparison to our first simulation where r=10 and the temperature is equal to 4.2 K, so in our case:

$$K_BT < 0.002(\frac{e^2}{C_\Sigma})$$

And for that reason the thermal effects are small. In our real case the jumps associated
With $n_0 \rightarrow n_0 \pm 1$ are no longer vertical jumps but rounded because of r$\neq \infty$

This effect is shown in the next Figure:
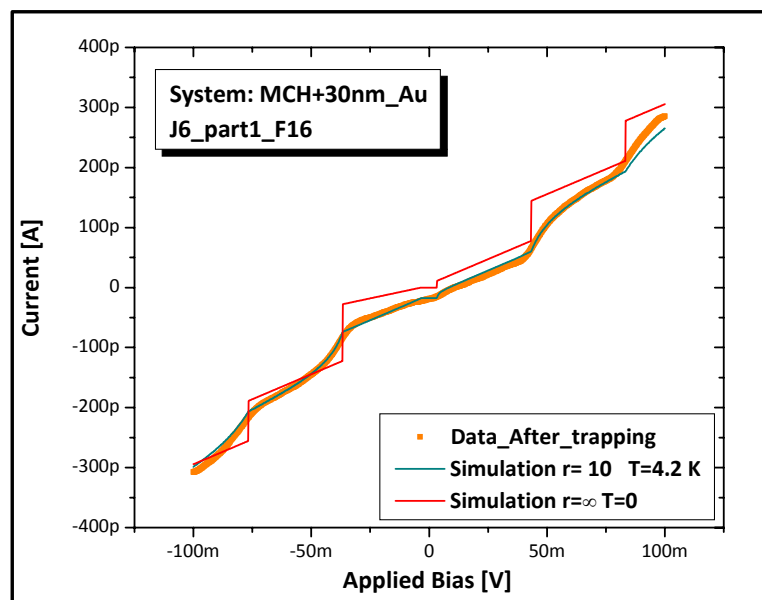
Fig 5.13 I-V characteristic of Coulomb blockade staircase effect: data and simulations. We see the effect in the ladder steps, induced by the ratio r (r=R2/R1) when the value of this parameter is both r=∞ or r=10.

5.3 Conclusion

In the experiments carried out through the thesis and by means of a soft trapping a two junction system Au/MCH/colloid/MCH/Au is created. Two are the effects observable in this system depending on the symmetry of our tunnel barriers.
On the one hand the Coulomb blockade behavior, which is dominant and appears when the two tunnel barriers have identical parameter ratio (R_1C_1=R_2C_2).On the other hand Coulomb blockade staircase behavior, which is dominant if a strong asymmetry exists in the parameter ratio that is, the product for the parameter junctions is very different (R_2C_2>> R_1C1).

Summary and Outlook

During this thesis a novel fabrication route for vertical nanogap devices has been presented. By laterally patterning an SOI wafer with a 20 nm buried oxide layer using optical lithography, conventional etching and metal deposition techniques nanogaps of separation 26 nm have been fabricated. TEM cross-sectional analysis have revealed a well defined material layer architecture suggesting the tailored design and fabrication of nanogap electrodes of desired shape.

To investigate the fabricated nanodevices *6-Mercapto-1-hexanol* (MCH) molecules have been placed on the nanoelectrodes by means of SAM process, and for bridging the 26 nm nanogap width, gold nanoparticles of different sizes in diameter have been placed, using a positive AC dielectrophoresis force. The successful parameters for a soft trapping have been found to be: AC Voltage using a square signal, amplitude of 4 V_{pp} and a frequency of 85 KHz applied during 180 seconds. After the achievement of a two-junction system (Au/MCH/Au/MCH/Au), by the soft trapping of nanocolloids of 30 and 60 nm of diameter, transport measurements are carried out in our devices. A visible current change in the range from 30 pA to 300 pA within the I-V characteristics measured at LHe temperature has been observed in a range between -100mV to 100 mV. Our measurements on nanogaps have given the evidence of a successful SAM and trapping process. A thoroughly study of I-V characteristics is also developed in the thesis and by means of the result analysis, effects such as Coulomb blockade and variation of the Coulomb blockade staircase are found. During the study of the variation of the Coulomb blockade staircase the parameters which define the two-junction system are calculated. A software simulation in comparison with the experimental data obtained in the laboratory, has provided the following values for the two-junction system are: C_2=4.45 aF, C_1= 4.45 aF , Q_0= -0.4166e, R_2= 300 MΩ and R_1=30MΩ.

For future projects a deeper electrical characterization of Oligophenylenevinylene (OPV) molecules such as OPV_3, OPV_5 and OPV_7, is presented as a very attractive idea. A further knwoledgment about the behavior of theses conjugated molecules, is seen as an approach for a real hybrid (semiconductor-molecular) system.

Another possibility for transport measurements in single conjugated molecules, would be the building of dimmers using a chemical process. Once theses dimmers structures are trapped between the electrodes by means of a dielectrophoretic force a charge transport study through this nanoparticle/molecule/nanoparticle bridge structure could be carry out. The creation of a hybrid system molecule-Au nanoparticle is an alternative, and once this system is chemically obtained and trapped between the electrodes, perform the electrical transport measurements through it.

Within the nanogap fabrication field, the development of narrower nanogaps is a desirable goal, so as in this way, the molecules are able to bridge the nanogap width by themselves, without the help of nanoparticle trapping. A possible solution for this achievement would be the usage of SOI wafers with a buried oxide width of 10 nm and the optimization parameters for the nanogap fabrication process.

Chapter 1

[1] Chad A. Mirkin "The Beginning of a Small Revolution" *Small 2005, 1, No. 1editorial essay.*

[2] N. J. Tao "Electron transport in molecular junctions" *Nature Nanotechnology, Vol1 December 2006.*

[3] Sebastian M Luber, Sebastian Strobel, Hans-Peter Tranitz, Werner Wegscheider, Dieter Schuh and Marc Tornow. Nanometre spaced electrodes on a cleaved AlGaAs surface. *Nanotechnology 16 (2005) 1182–1185; Luber et al.Small (2007).*

[4] Simone Maria Lingitz. Diplomarbeit: "Electronic Transport Investigations on Conjugated Molecules Based on Nanogap Electrode Devices". September 2006. Walter Schottky Institut (TUMünchen).

[5] Fan Zhang. Master thesis."Nanometer spaced electrodes for molecular electronics applications". November 2005. Walter Schottky Institut (TUMünchen).

[6] Sebastian Strobel , Kenji Arinaga, Allan Hansen and Marc Tornow Silicon-on-insulator vertical nanogap device for electrical transport measurements in aqueous electrolyte solution *Nanotechnology 18 295201 (5pp)(2207).*

[7] Robert J. Barsotti, Jr., Michael D. Vahey, Ryan Wartena, Yet-Ming Chiang, Joel Voldman, and Francesco Stellacci. Assembly of Metal Nanoparticles into Nanogaps .*Small 2007, 3, No. 3, 488 – 499.*

Chapter 2

[1] Iowa State University. Materials Science & Engineering Dept *web site.*

[2] www.steve.gb.com/images/

[3] Nobel Prize organization *website.*

[4] Electron Microscopy. Principles and Fundamentals. Edited by S. Amelinck, D. van Dyck, J. van Landuyt, G. van Tendeloo VCH .A Wiley Company.

[5] Nanoelectronics and Information Technology. Advanced Electronic Materials and novel devices. Second, corrected edition. Rainer Waser. *Chapter 10- Material removing techniques pages 249-53* (2005).

[6] City university of Hong Kong, Chapter 6: Etching *(web).*

[7] Microproccesing of Silicon on insulator substrates and biofunctionalisation of silicon dioxide surfaces for sensing applications in fluids. Karin Buchholz Vol 73. Editors G. Abstreiter, M.C Amann, M.Stutzmann, P. Vogl WSI, TUM (2006).

[8] Plasma Etching. Patrick Verdonck.

[9] http://www.ul.ie/~childsp/CinA/Issue53/issue53_files/main.htm.

Chapter 3

[1] Microproccesing of Silicon on insulator substrates and biofunctionalisation of silicon dioxide surfaces for sensing applications in fluids. Karin Buchholz Vol 73. Editors G. Abstreiter, M.C Amann, M.Stutzmann, P. Vogl WSI, TUM (2006).

[2] Nanoelectronics and Information Technology. Advanced Electronic Materials and novel devices. Second, corrected edition. Rainer Waser. *Chapter 10- Material removing techniques page 251*(2005).

Chapter 4

[1] J. Christopher Love, Lara A. Estroff, Jennah K. Kriebel, Ralph G. Nuzzo, and George M.Whitesides. Self-Assembled Monolayers of Thiolates on Metals as a Form of Nanotechnology *.Chem. Rev. 2005, 105, 1103-1169.*

[2] Frank Schreiber. Structure and growth of self-assembling Monolayers. *Progress in Surface Science 65 (2000) 151-256.*

[3] Institute of Bioelectronic and Molecular Microsystems *website*. Schools of Electronic Engineering and Computer Science. University of Wales, Bangor.

[4] Robert J. Barsotti, Jr., Michael D. Vahey, Ryan Wartena, Yet-Ming Chiang, Joel Voldman, and Francesco Stellacci. Assembly of Metal Nanoparticles into Nanogaps *Small 2007, 3, No. 3, 488 – 499.*

[5] Jeong-Seok Na, Jennifer Ayres, Kusum L Chandra, Changwoong Chu, Christopher B Gorman and Gregory N Parsons. Conduction mechanisms and stability of single molecule nanoparticle/molecule/nanoparticle junctions. *Nanotechnology 18 (2007) 035203 (8pp).*

[6] http://www.sc.ehu.es/sbweb/fisica/fluidos/tension/capilar/capilar.htm

[7] BBInternational *web site*.

Chapter 5

[1] Leo P, Kouwenhoven, Charles M.Marcus, Paul L, Mceuen, Seigo Tarucha, Robert M. Westervelt, and Ned S.Wingreen. Electron transport in quatum dots. To be published in the proceedings of the Advanced Study Institute on Mesoscopic ElectronTransport, edited by L.L. Sohn, L.P. Kouwenhoven, G. Schön (Kluwer 1997).

[2] H. van Houten, C. W. J. Beenakker, and A. A. M. Staring. Coulomb-Blockade Oscillations in Semiconductor Nanostructures. Published in Single Charge Tunneling, edited by H. Grabert and M. H. Devoret, NATO ASI Series B294 (Plenum, New York, 1992).

[3] J. G. A. Dubois , J. W. Gerritsen , S. E. Shafranjuk , E. J. G. Boon , G. Schmid and H. van Kempen. Coulomb staircases and quantum size effects in tunnelling spectroscopy on ligand-stabilized metal clusters. *Europhys. Lett, 33 (4), pp. 279-284 (1996).*

[4] Mesoscopic Phenomena in Solids, edited by B. L. Altshuler, P.A Lee ,and R.A Webb (Elsevier, Amsterdam, 1991) p 173 D.V Averin and K.K Likharev.

[5] E. Hanna and M.Tinkham.Variation of the Coloumb blockade staircase in a two- junction system by fractional electron charge. *Physical review B ,Volume 44, number 11 (1991).*

[6] M. Amman and R. Wilkins. Analyticsolution for the current-voltage characteristics of two mesoscopic tunnel junctions coupoled in series. *Physical Review B Volume 43, number 1 (1991).*

[7] Nanoparticles and nanogaps: controlled positioning and fabrication Roman Krahnea;, Tali Dadoshb, Yoav Gordina, Amir Yacobya, Hadas Shtrikmana, Diana Mahalua, Joseph Sperlingb, Israel Bar-Josepha Physica E 17 (2003) 498 – 502.

[8] David L. Klein and Paul L. McEuen An approach to electrical studies of single nanocrystals Applied Physics Letters -- April 29, 1996 -- Volume 68, Issue 18, pp. 2574-2576.

[9] Simple and controlled fabrication of nanoscale gaps using double-angle evaporation
Akinobu Kanda, , Mitsuhiro Wada, Yoshihisa Hamamoto and Youiti Ootuka *Physica E: Low-dimensional Systems and Nanostructures Volume 29, Issues 3-4, November 2005, Pages 707-711.*

 [10] Software developed by A.Korotkov and K.K Likharev (1992).

Acknowledgments

This work would have not been possible without the support of many persons whom I would like sincerely to thank to:

➢ **Dr. Félix Martínez Viviente** for his great idea of recommending me to come to the WSI and for his important support and trust in me.

➢ **Dr.Joan Garcia Haro** for his always wise advices, support and very useful help during all my studies in the Universidad Politécnica de Cartagena.

➢ **Especially I would like to thank to my family and friends**. My parents: Pepe and Isabel and my grandmother Ginesa, who have accompanied me in every moment in my life during these 24 years and from Cartagena have understood and supported all my decisions. I am completely grateful for their love and inestimable encouragement. All my friends in Munich and in Spain: Irene, Vivien, Veronica, Virginia, Paola, Jose, Santy, Elena, Jesus, Ainhoa, Celia, Rebeca, Beatriz, , Inés, Juanmi, Luis, Katy, Mayte , Marta, Carolina, Ana Mostaza and all the people who encouraged me to come to Munich and to continue with my German experience.

➢ **All my teachers** in the Escuela Técnica Superior de Ingeniería de Telecomunicación in the UPCT, because all of them are great persons and great teaching professionals. And also I would like to thank to Juan and Serafín, for being probably the best English teachers around the world.

➢ **Erasmus foundation and Universidad Politécnica de Cartagena** for allowing and supporting the student mobility.